Automated Monitoring of River Ice Processes from Shore-based Imagery

Saber Ansari

Thesis submitted to the
Faculty of Graduate and Postdoctoral Studies
In partial fulfillment of the requirements
for the Master of Science degree in Civil Engineering

Department of Civil Engineering

Faculty of Engineering

University of Ottawa

Abstract

Ice plays an important role in hydraulic processes of rivers in cold regions such as Canada. The formation, progression, recession and breakup of river ice cover known as river ice processes affect river hydraulics, sediment transport characteristics as well as river morphology. Ice jamming and break up are responsible of winter flash floods, river bed modification and bank scour. River ice cover monitoring using terrestrial images from cameras installed on the shores can help monitor and understand river ice processes. In this study, the benefits of terrestrial monitoring of river ice using a camera installed on the shore are evaluated. A time-lapse camera system was installed during three consecutive winters at two locations on the shores of the Lower Nelson River, in Northern Manitoba and programmed to take an image of the river ice cover approximatively every hour. An image analysis algorithm was then developed to automatically extract quantitative characteristics of the river ice cover from the captured images. The developed algorithm consists of four main steps: preprocessing, image registration, georectification and river ice detection. The contributions of this thesis include the development of a novel approach for performing georectification while accounting for a fluctuating water surface elevation, and the use of categorization approach and a locally adaptive image thresholding technique for target detection. The developed algorithm was able to detect and quantify important river ice cover characteristics such as the area covered by ice, border ice progression and ablation rate, and river ice break up processes with an acceptable accuracy.

Acknowledgements

First and foremost I would like to express my sincere appreciation and gratitude to my thesis advisor Dr. Colin Rennie, for all his mentorship, continuous support and generosity during my Master studies. I am grateful for his many contributions to my program of research, including his precious technical advices, as well as involving me in a leading edge research project and giving me the opportunity to collaborate with his extensive network of research professionals nationally and internationally on interdisciplinary projects. I would also like to acknowledge my co-supervisor, Dr. Ousmane Seidou. I wish to sincerely thank for his invaluable support and feedback on my work, and providing me with precious programming advices. I would also like to thank Hatch Corporation Ltd., Manitoba Hydro, and Natural Sciences and Engineering Research Council for their support and funding. My special thanks are extended to Dr. Jarrod Malenchak for his comments and feedbacks on publications and giving me access to the requested data. I would also like to thank Nathan Lambkin and his crew from Manitoba Hydro for all their help and contributions during field measurements and camera installations. I would like to acknowledge the faculty and support staff of the Civil Engineering Department for their support in my academic program. I would also like to thank my dearest friend and colleague Soheil Gharehaghaji Zare for his help and support during my studies. Finally, special thanks to my Family. Words cannot express how grateful I am to my parents, Alireza and Gohar, for all the sacrifices they've made which sustained me thus far. Thanks and love to my one and only sister, Sanam, for her love and encouragement and to my closest friend, Reza, who I can call brother. Last, but never least, I would like to express my appreciation to my beloved wife Behnaz. Her endless support, encouragement, patience and unwavering love, is the bedrock of the life that I always wanted to establish. Thanks for being who you are.

Dedication

This thesis is dedicated to the memory of my dear father, who has been my constant source of inspiration, Dada this is for you.

Table of Contents

List of Tables

List of Figures

List of symbols and abbreviations

Acoustic Doppler Current Profiler	ADCP
Camera coordinates	C
Coordinates of a point in camera coordinates system	P_c
Digital Elevation Model	DEM
Edge indicator function	g(x,y)
Field of View	FOV
Focal length of the camera	f
Geographic Information System	GIS
Ground Control Points	GCPs
Horizontal axis of the camera coordinate system	U
Image definition	$I(x, y)$
Image panel width	w
Joint Photographic Experts Group Image file format	JPEG
Limestone Generation Station	LGS
Lower Nelson River	LNR
Multi-Functional Acoustic Water Column Profiler	MF- AWCP
Point in world coordinates system	P_w
Projection of $\vec{N}$, on the horizontal plane	$\vec{N}_{xy}$
Root mean square error	RMSE
Target Point	T
Target point elevation	T_z
Target surface equation	$T(x, y)$
Translated point in camera coordinates	P_t
Vertical axis of the camera coordinate system	V
Viewing vector	N
Viewing vector elevation	N_z
Weighting parameter	α

Chapter 1
Introduction

1.1. Background

River ice generation during the winter occurs in several regions of the World and has several direct and indirect impacts on human's social and economic life as well as on the rivers' morphology and ecosystems. A non-exhaustive list of affected industries includes the winter recreation industry, the fishing industry, fluvial transportation, hydropower generation and water supply. River-ice induced floods are known to have a high socioeconomic cost (Beltaos 1984; Prowse and Beltaos 2002) and wide ecological and environmental influences (e.g. Chambers 1994; Prowse 2001; Smith and Pearce 2002 Lind, Nilsson, and Weber 2014). River ice also affects the rate of sediment transport which in turn can affect fish habitat and siltation in reservoirs. Despite these widespread impacts, there is still insufficient knowledge about ice generation and ice cover evolution in winter, partly because of data unavailability for model calibration and validation. A relatively little number of studies have reported continuous monitoring of river ice and most of these researches utilized satellite imagery for the monitoring purpose (e.g. Das et al. 2015). Among them, an even smaller number of studies have also reported terrestrial monitoring of river ice cover (Bourgault 2008).

This thesis study aims at assessing a river ice monitoring technique based on terrestrial photogrammetry. It is part of a comprehensive research program being conducted on Lower Nelson River (LNR), Manitoba- Canada since 2012 by a consortium of institutions (the University of Ottawa, Manitoba Hydro, the University of Manitoba, Hatch inc.). The general

objective of the larger study is to get a better understanding of river ice formation and break-up processes and its influence on river hydraulics. The LNR is a regulated semi-alluvial river that drains Lake Winnipeg, to Hudson's Bay flowing in northern Manitoba, after spilling out into several other lakes (Newbury, 1986; Pip 1992). The river ice monitoring was conducted in a 102 km reach of LNR, between Limestone Generating Station (LGS) and Gillam Island (Figure 1-1). Two locations along the LNR were selected to examine the effects of river ice cover over river hydraulics and sediment transport.

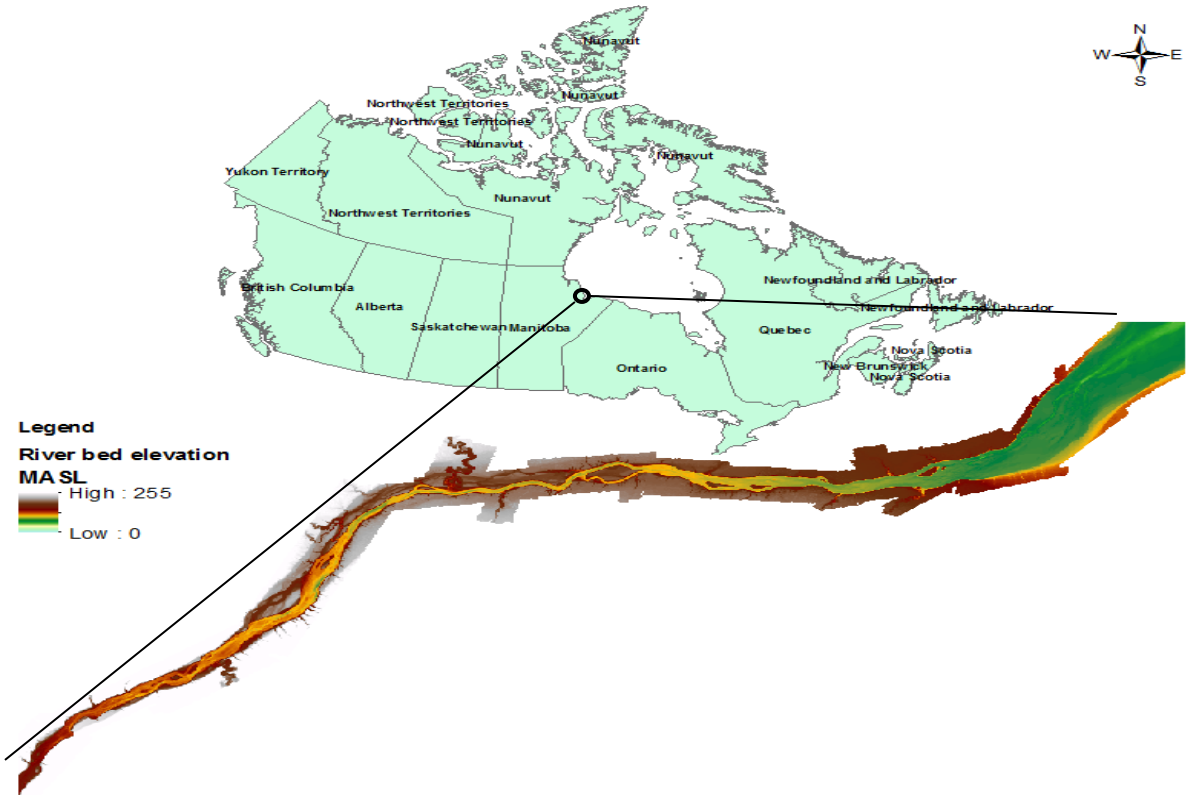

Figure 1-1 Study Area, Lower Nelson River, Manitoba, Canada

1.2. Research Questions

The specific questions this thesis tried to answer are the following:

- Can river ice cover characteristics be automatically extracted from still camera images?
- What factors affect ice cover characteristic extraction from still camera images?
- What are the best image analysis algorithms for river ice cover characteristic extraction from still camera images?
- How accurate are the extracted ice cover characteristics?

1.3. Methodology

Computer vision algorithms for target detection were utilized (and sometimes adapted) for the automatic extraction and georeferencing of ice covered areas in the time series of images acquired by the time lapse cameras. The developed automated shore-based image analysis algorithm includes four steps: preprocessing, image registration, rectification, target detection. As the first step, different image processing techniques and definitions are used to enhance the quality of the images if possible, and discard images which's quality is too poor. Discarding poor quality images make the algorithm faster and makes the analysis of the final results easier. At the second step (image registration), the effect of camera movements is removed so that a given pixel always represents the exact same point in the real world. At the third step (image rectification), the algorithm proposed by Corripio et al. (2004) was modified and applied to the images captured at two location along the LNR. The algorithm uses intrinsic and extrinsic characteristics of the camera to superimpose the Digital Elevation Model (DEM) map of the camera field of view on an image to assign correct coordinate information to the pixels of the image. At the final step (river ice detection), a locally adaptive image thresholding method was

adapted to detect river ice cover, and perform the final calculations to quantify ice cover characteristics.

1.4. Novelty

As previously mentioned, the main goal of this study was to employ terrestrial oblique imagery to monitor river ice cover and quantify important river ice cover characteristics. Only a small number of studies have reported shore-based terrestrial monitoring of river ice cover (Bourgault 2008; Jędrzychowski & Kujawski 2014). None of these studies used an automated image analysis algorithm that is able to perform image quality processing, registration, georectification and detection. Bourgault (2008) presented a successful method to georectify shore-based images of St. Lawrence River but did not introduce a method of automated river ice detection. Furthermore Ground Control Points (GCPs) played an important role in his rectification method. However, in this study, the rectification method introduced by Corripio (2004); Härer et al. (2013) was modified for the changing surface of the river. Unlike the georectification technique applied in previous studies, the modified georectification technique is not dependant on GCPs. This advantage makes the technique suitable for monitoring of river ice in remote places. Furthermore, an edge sensitive variational image thresholding technique (Ray & Saha 2006) was adapted for river ice cover detection. The ice detection technique used in this algorithm was able to detect ice in the images taken with a camera without any filter. The detection subroutine employed in this algorithm is more accurate compared to similar studies (Jędrzychowski & Kujawski 2014). As a final unique achievement of this study, the presented algorithm extracted the quantity of river ice cover area, border ice generation and recession rate. For the first time, the presented algorithm can perform a robust and automatic rectification, detection and calculation of river ice cover characteristics based on oblique terrestrial sets of images.

From a practical point of view, this study is the first to generate hourly time series of ice cover characteristics. While the use of these time series for the validation of ice cover evolution models is beyond this thesis, it is definitely a valuable contribution that will lead to more reliable models and therefore better insight on river ice processes.

Chapter 2

Literature review

Studies on river ice cover dynamics and its influences on the environment are relatively new and early studies revert to Pariset & Hauser (1961) and Shulyakovskii (1963). River ice and ice processes were afterward studied by a few authors (Carey, 1967; D. G. Smith 1979; Calkins, Deck, and Martinson 1982; Ashton, 1986; Ferrick and Calkins 1996; S. Beltaos 2001; Shen 2003; Best, Ettema and Zabilansky 2004; Pavelsky and Smith 2004; McNamara, and Liberty 2005; S. Beltaos 2011; Yang and Wang 2015; Ghareh et al. 2016). The three main topics of these studies were the influence of river ice cover over the hydraulic characteristics of the river (e.g. Carey, 1967; Calkins, Deck, and Martinson 1982; Ferrick and Calkins 1996; S. Beltaos 2001; S. Beltaos 2011; Ghareh et al. 2016) the effect of ice cover on river morphology (e.g. D. G. Smith 1979; Best, Ettema and Zabilansky 2004; Pavelsky and Smith 2004; McNamara, and Liberty 2005), and finally the effect of ice on sediment transport (e.g. Moore et al. 2013; Zare et al. 2014; S. Beltaos 2016; S. Beltaos and Burrell 2016) and water quality (e.g. Ranjie and Huimin 1987; Tang et al. 2016).

This study focuses on off-shore terrestrial monitoring of river ice cover in Lower Nelson River. Two cameras were mounted on two different locations along the LNR to monitor river ice cover processes. The time series images from these two locations were then analyze using the developed automatic shore-based terrestrial imagery algorithm. The following sections present some background information on both river ice processes and computer vision methods and techniques used in the developed algorithm.

2.1. River ice

River ice processes include ice generation, growth, transportation, accretion, dissipation, and ablation of various forms of ice. Complex hydrodynamic, mechanical and thermal processes as well as hydro-meteorological conditions and stream morphology are involved in these processes (Wang et al. 2016). The first phase of river ice formation starts when air temperature drops to the freezing point (usually in mid-fall or winter). Air temperature drop is followed by water supper-cooling and frazil ice formation. Various types of ice are generated depending on flow characteristics. Skim ice is formed in the case of slow flow, while frazil ice forms on the water surface and the water underneath in high velocity flow when turbulence causes mixing. Frazil ice can grow in size and quantity up to the whole depth of the flow. Skim ice generated close to the banks of the river may lead to border ice generation when water is stationary, while mobile skim ice may join the process of the river surface ice run to the downstream of the river. Figure 2-1 illustrates the process of ice freeze up based on travel time and the turbulence intensity in the water (Hammar et al. 2002). It shows that stationary skim ice is generated on calm water. This phenomenon usually occurs in lakes, ponds and the low velocity portions of rivers. On the other hand, when the flow is more turbulent, slush ice web forms and transforms into ice blanket or the slush pans. The increase of slush ice concentration through time eventually produces stable ice cover by the formation of more ice pans and ice floe sheets. On a more turbulent flow generated stratified frazil ice and well mixed frazil ice can transform into slush run of granular ice and slush balls respectively.

Growth of skim ice on the borders of a river forms the static border ice, and leads to the upstream progression of the cover. This progression continues as long as conditions favorable to the ice cover thermal growth exist. Thermal growth and decay of river ice cover occurs when the

conditions favorable to the formation and ablation of the river ice cover reaches to the stability. Detached river ice covers travel downstream of the river through undercover transport and lead to accumulation.

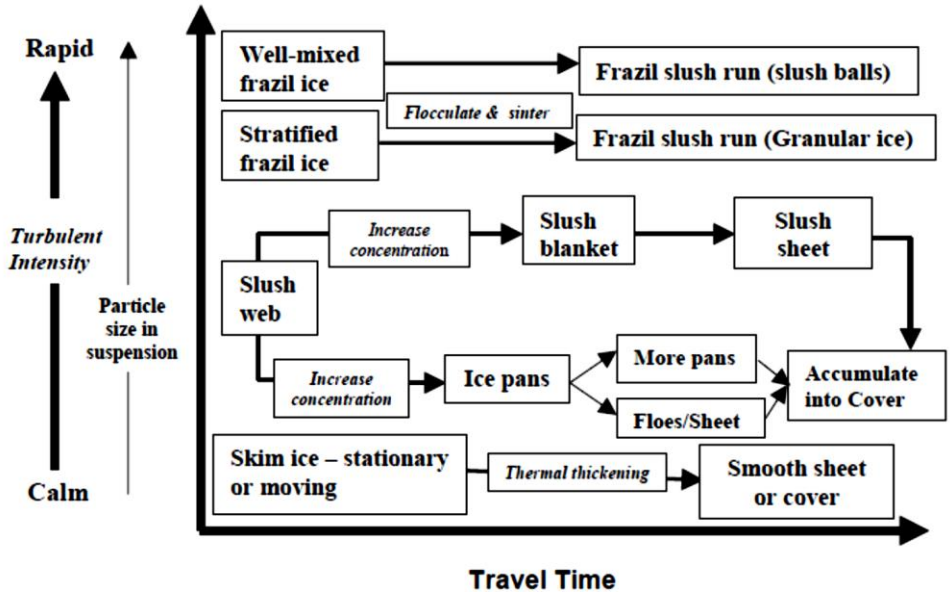

Figure 2-1 Freeze up ice formation processes (Hammar et al. 2002)

Figure 2-2, illustrates river ice processes described as by Shen (1996). Frazil ice which usually forms in turbulent water flow and is the origin of the most types of river ice cover. In turbulent super-cold water, frazil ice actively travels in transversal and vertical directions and attaches to any object, forming different kinds of river ice cover. The mixed super cold turbulent water leads to the formation of frazil ice crystals. Many scientists believe that the primary mechanism of frazil ice formation is the secondary nucleation on ice particles (Hicks 2009). Frazil ice particles can be found in different size and shape and usually with in only a few millimeters. These particles are sometimes entrained to the bottom of the river, forming anchor ice by attaching to river bed or the objects on the bed (Shen, 1996). Anchor ice is one of the most important types of

river ice, that can affect hydraulic as well as ecological characteristics of the river (Prowse 2001; Kerr, Shen, and Daly 2002). On the other hand, frazil ice particles can accumulate or flocculate to form the frazil slush, which after reaching to a specific size start to float on the surface of the river creating floating ice known as “pancake ice”. As the surface concentration of river ice increases, floating ice pans travel to the downstream of the river forming ice rafts by integrated freezing of ice pans. Some of the downstream traveling ice pans accumulate along the river banks forming “shore ice”. Generation of this type of shore ice occurs when the average depth velocity of water is less than 0.4 m/s (Shen, 1996). Accumulation of shore ice induced by congestion of river ice and cessation of their movements leads to “Jamming” or “bridging” phenomenon. Ice jams occur at tight bends and locations where stream narrows with an increase of ice concentration, several models have been developed to simulate dynamic transport and evolution of ice jams (Tao & Li 2016). Border growth of river ice eventually causes the constriction of the stream and further growth of cover by edge to edge accumulation of downstream flowing of ice pans. The upstream growth of river ice cover which occurs because of the constriction of the stream is called “Juxtaposition”. Upstream progression of river ice stops when river ice velocity increases to a critical threshold, sweeping ice floes underneath the ice cover. This in turn leads to increase in the thickness of the river ice cover, which is called “Hydraulic thickening”. Previous researches and field observations suggest a Froude Number value of about 0.09 (Sun & Shen 1988), for hydraulic thickening to occur.

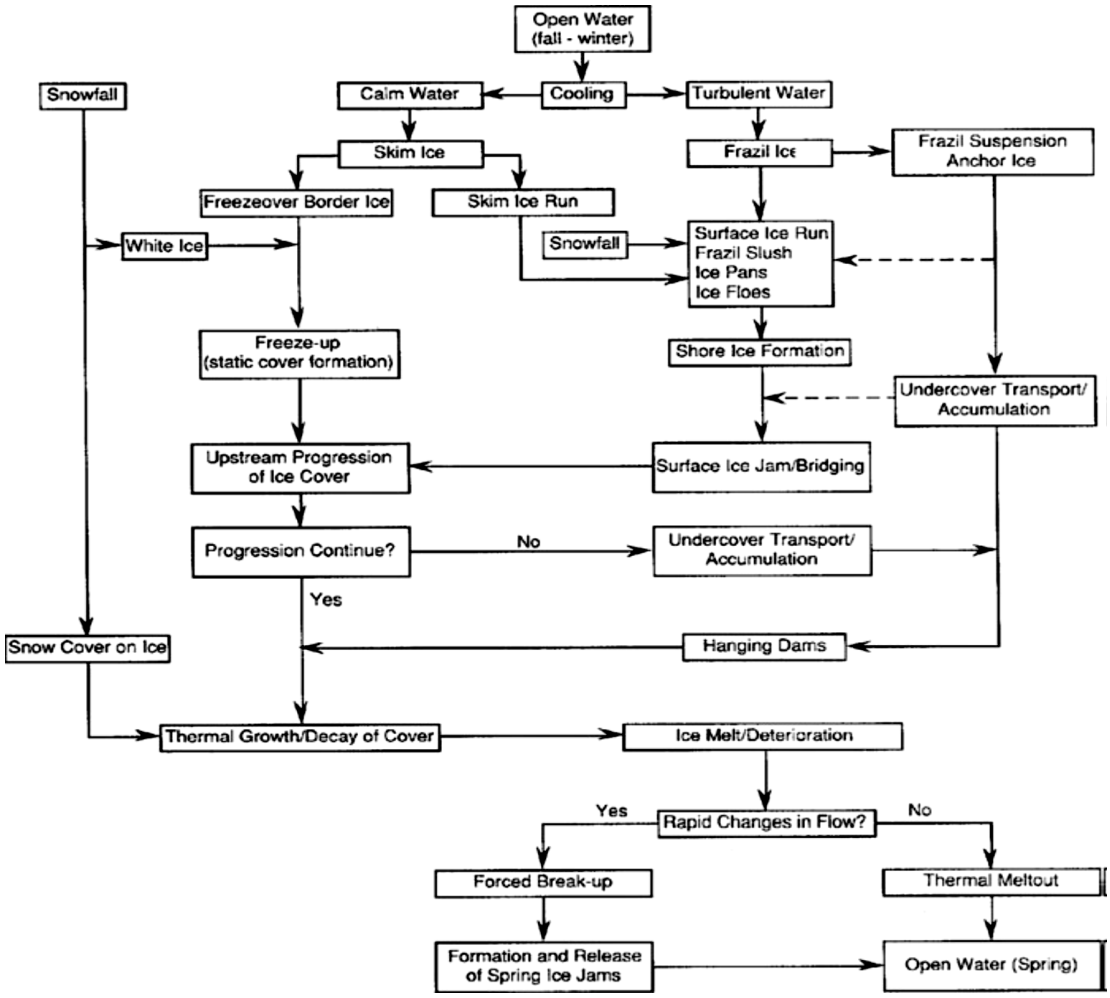

Figure 2-2 River ice processes (Shen, 1996)

River ice cover withstands several forces, such as current drag, wind drag and the weight component of the cover along the river (Shen, 1996). If the induced forces exceed the resistance of the cover, it will collapse or shove. Figure 2-3 shows the "hummocky" ice generated through shoving process on LNR. Stabilization of such accumulated ice drastically increases the ice cover's thickness and strength, leading to water level rise and in some cases overbank flooding. The upstream progression of river ice cover stops at a cross section with higher velocity, triggering the formation of the open water sections along the river Figure 2-3. Open water patches tend to remain open during winter, producing frazil ice that travel downstream of the

river through an undercover transport. The ice particles generated in an open water patch are in the form of frazil granules due to the high velocity of the current. The undercover transported frazil ice particles form localized accumulation of frazil beneath the river ice cover. Localized undercover accumulation of the frazil particles is called “hanging dam” or “frazil jam”. Frazil jams can potentially cause river ice cover break-up subsequent to the increase of water level which is due to the excessive accumulation of ice. Comprehensive researches have been conducted over frazil jam, for a better understanding of frazil jam evolution and its effect on water level rise (e.g. Sui et al. 2002).

Figure 2-3 Hummocky ice formation (left) and open water patch (right) on Lower Nelson River, Northern Manitoba, February 2013, courtesy of S.G. Zare

The thickening of the stable ice cover continues during winter both above and beneath the surface through different procedures. Undercover thickening of the river ice cover occurs in the condition of thermal heat loss, whereas additional ice cover may also be added to the surface of the cover when there is a snow layer covering the river ice cover. Seeping water through cracks of ice cover saturates the under layer of the snow cover helping the layer to freeze and join the consolidated ice cover.

Breakup occurs either through gradual melting process called “thermal deterioration”, or sudden breakup due to increased river discharge called “dynamic breakup”, but most often by a combination of both processes (Ashton 1978). The break up mechanism may vary in different rivers and in various sections of a river. Initial melting of stable river ice cover begins on early spring, as the air temperature starts to rise. Increase of water temperature and continuous heat exchange between water and ice cover through the turbulent heat transfer leads to initial decay and deterioration of ice cover on both surfaces of the cover. Thermal deterioration leading to the thinning process of the ice cover is shown in figure 2-4. The thinned and weakened river ice cover becomes sensitive to dynamic forces and even a limited increase in river discharge can lead to initial cracks on cover, which ultimately leads to final breakup and removal Figure 2-4. Ice thickness, degree days of thaw, and also the increase in the water stage are the most important governing parameters of premature or mechanical breakup (Ashton 1978).

Figure 2.1-4 Smooth river ice cover due to thermal thinning (left), ice cover removal (right) on Lower Nelson River, Northern Manitoba, May 2013

2.2. Terrestrial imagery

Terrestrial imagery is a cost effective and convenient method for data acquisition, measuring and monitoring land surface variables. This monitoring technique is widely used in earth sciences

and engineering. Large amount of continuous data can be gathered using terrestrial imagery techniques with minimal effort and cost. Terrain photogrammetry is widely used in earth science related projects and its popularity is increasing due to the large amount of data that can be acquired, and the fact it can be used in remote places. It was used for instance to monitor glaciers in cold mountainous regions, (Wiessmann et. al. 2012; Kaufmann 2012), water management (Barker et al. 1997), data collection on vegetation phenology (Sonnentag et al. 2012; Zhou et al. 2013; Keenan et al. 2014; Beamish et al. 2016), monitor land cover evolution (Zier and Baker 2006; Michel, Mathieu, and Mark 2010; Niraula et al. 2013; Schmidt et al. 2015), and for data acquisition in volcanology (Major et al. 2009). Terrain photogrammetry has also been used in river ice monitoring (Bourgault 2008), as an aid for navigation and for predicting and preventing ice jams and floods. In another study, Jędrzychowski and Kujawski (2014) used terrestrial monitoring of river ice as an assessment method for river ice cover, used for transportation.

Gathering data and monitoring in field parameters of a remote site through photography is a useful and practical idea; however, the data cannot be fully exploited if it is not georeferenced through georectification. Georectification is the digital alignment of an image with the map of the same area. The term "Georectification" mostly was used for georeferencing of satellite or aerial images. However with the recent increase in the application of terrestrial imagery and the developing methods of georeferencing, this term is also used for land based oblique images. Georectification is the most important step in the analysis procedure of oblique photogrammetry, being a crucial step in extracting quantitative results. Four major steps in georectification of oblique terrestrial images are (Pawlowicz 2003):

1- Translation of the pixel locations into camera viewing vector, relative to the central axis of the camera.

2- Application of the appropriate rotational equations through all three axes of “x”, “y” and “z”.

3- Determination of a relationship between viewing vector of the camera and the ground surface.

4- Conversion from coordinates of ground point to true ground coordinates.

Different georectification methods have been used with various camera models and equations for translation, rotation and conversion of the image pixels to the true world coordinates (Holland et al. 1997; Pawlowicz 2003; Corripio 2004; Bourgault 2008; Härer et al. 2013; Messerli and Grinsted 2015). These methods require accurate information about the intrinsic and extrinsic camera characteristics, such as horizontal and vertical position of the camera as well as camera view angle from north and dip horizontal angle, camera field of view and focal length. However, to increase the validity of the rectification method some methods utilized Ground Control Points (GCPs) to optimize the rectification equations (i.e. Bourgault 2008).

Another important step in terrestrial imagery, is the detection of the objects and variables in the images. This can be done manually by a human, but is more and more done through computer vision techniques such as target detection and image segmentation. The next section of the thesis presents some basic notions in computer vision. The specific techniques used in this work are presented in the third section of this thesis.

2.2.1. Computer vision

Computer vision is a novel field of research which uses computers to extract accurate information from digital images, using different methods for processing, analyzing and interpreting the images. Computer vision tries to come up with the computational methods that

mimic human vision system and link these methods and techniques to automatic computer analysis for different tasks and analysis (Huang 1997). In other word, "computer vision" is the science of developing algorithms and processes which allow computer to see. The idea of extracting 3D geometric information from 2D perspective views, initially presented in a MIT PhD thesis by Larry Roberts. This idea has been developed by several researchers throughout years and recently a broad application spectrum can be defined for computer vision such as: autonomous vehicle, robotics, surveillance, and etc. Computer vision applies different methods of image analysis such as, image processing (quality enhancement of the images), photogrammetry (calibration of the camera and taken images to acquire different information from variables in the images), pattern recognition (learning patterns for classifying or analyzing data) and computer graphics (rendering a virtual scene), human/computer interfaces (methods of interacting between computers and human.

Image processing is the procedure of processing images using mathematical and geometrical operations. Mathematical tools used in image processing include, linear algebra, vector calculus, Euclidean geometry, projective geometry, differential geometry, differential equations, numerical analysis, and probability and statistics. In image processing usually processing of digital images is the main focus, however analogue and optical image processing is also possible (Burge, 2008).

In the remainder of the, section definition of some of the basic terms in image processing used in the thesis are presented.

Image Formation: A simple model of the camera and how an image is formed on camera panel is presented in figure 2-5. Assuming a thin lens, and that its optical axis is perpendicular to the image plane the following lens law is applicable:

$$\frac{1}{u}+\frac{1}{v}=\frac{1}{f} \qquad \textbf{[1]}$$

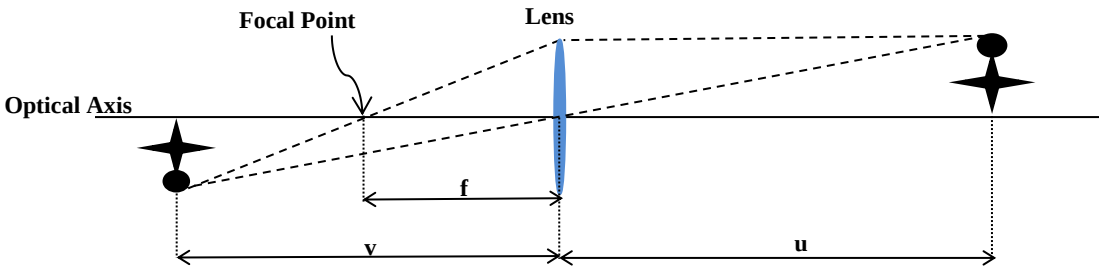

Figure 2-5 Fundamental equation for lens model

Focal Length: Distance between camera lens and the focal point. This parameter is a measure of how strongly the lens converges the light.

Angle of view: The angle of projected subject area on camera panel using a lens (Figure 2-6).

Field of view: Area visible by camera (Figure 2-6).

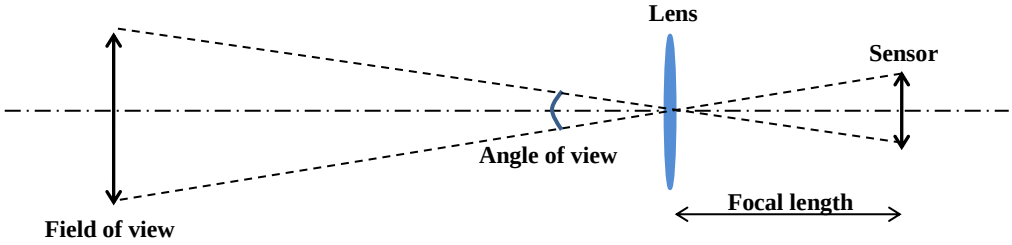

Figure 2.2-6 Field of view, angle of view and focal length

Digital Image: A numerical representation of a two dimensional image. A digital image usually consists of pixels.

Pixel: The smallest controllable element of the picture represented on the screen.

Binary Image: Images with pixel intensities of either zero or one. Binary image is normally black and white with pixel intensities of "1" and "0", respectively.

Color Image: Human eye is capable to detect approximately 350000 colors. All visible colors are combination of three main colors, that are red, green and blue (RGB). In a color image, a specific band is dedicated for each color. Color images are either *8-bit Color Images, or 24-bit Color Image.*

24-bit Color Image: **C**olor component intensity is stored as an 8-bit integer. Therefore considering 3 different colors; each pixel requires 24 bits for a complete coverage of the colors visible for human eye. The draw-back of the 24 bit color images are the storage they need.

8-bit Color Image: In 8-bit color images, the color of each pixel is stored in 8 bit pixels, so the number of the colors represented by an 8-bit color image is restricted to 256.

Grayscale Images: An image that the colors of all image pixels are shades of gray. In a grayscale image, the red, green and blue components of the pixels all have equal values.

Edge and Edge Detection: Places in an image with strong intensity contrast are called edges. Since strong variations in pixel intensity contrast usually occur in the boundaries of the objects in an image, therefore edge concept and edge detection is a very important and common tool in the area of feature detection. Many edge detection methods are being used to detect the sudden

changes of pixel intensity. These methods are categorized to two different groups; “search” and “zero crossing” based methods. The first step in search based methods is to compute a measure of edge strength, which is a first order derivative and then searching for the local maximum. On another hand in zero crossing based methods a search for zero crossing is performed in a second order derivative.

Canny edge detector: A multi-stage edge detection algorithm developed by (Canny 1986). This algorithm simplifies the edge detection by elimination of weak edges not connected to the stronger ones. Figure 2-7, shows the canny edge detector operator applied to an image of the time series.

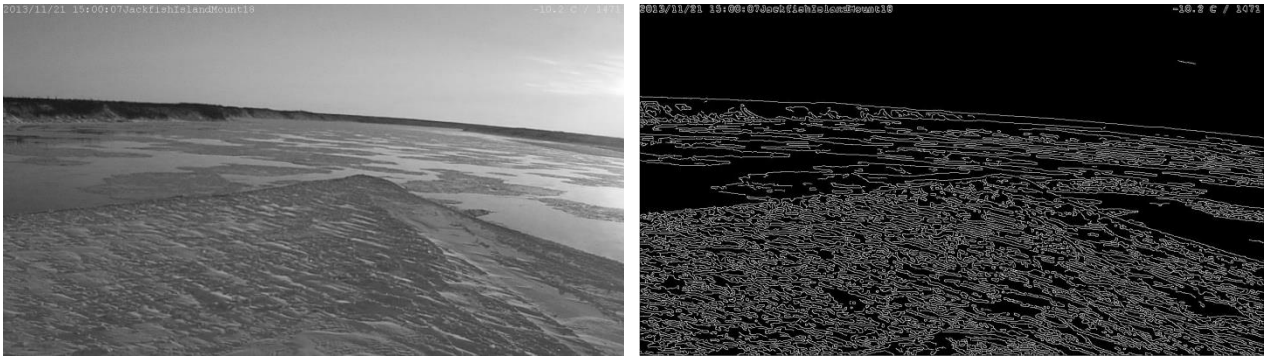

Figure 2.2-7 Canny edge detector operator applied to an image of Lower Nelson River, Jackfish Island site

Image Registration: The process of transforming different images to a unique coordinates of a reference image. Image registration is used for comparing two or a set of images with each other, e.g. medical imaging. In this project image registration was used to transfer all images of a time series to the coordinates of a reference image, to rectify the discrepancies caused by camera movements. Image registration algorithms can be categorized into two main groups, “Intensity based” and “Feature based”. Intensity based methods align the time series images to the reference image by comparing intensity patterns in images and the reference image via

correlation metrics. In feature based techniques images are aligned using the correlation between corresponding features.

Functional: is a function from the vector space to its corresponding scalar values, in other words it is a function that takes a vector and returns a scalar.

Variational principle: A logic principle used in the calculus of variations, that finds functions which extermize the value of quantities that depend upon those functions (Kristály, Alexandru, Rădulescu, & Varga, 2010).

Chapter 3

Journal Paper

Automated Monitoring of River Ice Processes using Shore-based Imagery

S. Ansari[1], C. Rennie[1], O. Seidou[1], J. Malenchak[2], S. G. Zare[1]

[1]Department of Civil Engineering, University of Ottawa Ottawa, ON, K1N 6N5
[2]Section Head, Ice, and Environmental Engineering, Department of Water Resources Engineering, Manitoba Hydro, Winnipeg, Manitoba, Canada

Abstract

River hydraulics is drastically influenced by the presence of river ice, which inevitably occurs in cold regions. Terrestrial monitoring of river ice, using a time-lapse camera system on the Lower Nelson River, northern Manitoba, Canada, was conducted for a comprehensive study of the effects of river ice cover on hydraulic characteristics. An automated image processing algorithm was developed to analyze the time series of terrestrial images. The presented image processing algorithm consists of four main discrete steps working in coordination with each other: preprocessing, image registration, geo-rectification, target detection and final quantitative river ice cover calculations. The developed algorithm was able to detect and quantify important river ice cover characteristics such as the percentage of area covered by ice, the location of the leading edge, and the speed of border ice growth and recession. Potentially, these observations may be used to improve the ice formation and break-up algorithms in river ice models.

Key words: river ice, terrestrial photogrammetry, shore-based

3.1. Introduction

Frozen rivers are valuable economic, social and recreational resources of cold regions. Presence of river ice cover, as a common element of these rivers, can drastically affect various river flow characteristics as well as socioeconomic aspects of the region. Various studies on river ice cover have indicated its influences on river hydraulic characteristic elements such as composite hydraulic resistance (Ghareh Aghaji Zare, et al. 2016a), and boundary shear stress (Ghareh Aghaji Zare et al., 2016b). On the other hand, there are several other studies showing the influence of river ice cover over water quality as well as mixing ability and transportation (P.A. Chambers, et. al. 1993; Ranjie & Huimin 1987; Tang et al., 2016). River ice cover can also significantly influence the morphology of rivers (Smith 1979), channel stability (Ettema & Zabilansky 2004), and sediment transport (Beltaos & Burrell 2016); hence, studying river ice regime and its processes in cold regions is a vital factor in river engineering and environment and ecosystem sciences. Results of such study can also be used in efficient management of water resources and/or hazardous events.

Oblique terrestrial photogrammetry has been introduced as an art, science and technology of gathering information from physical objects and the environment of remote places where data acquisition is a challenging task. In several studies of various fields such as glaciology (Kaufmann 2012), watershed management (Barker et al. 1997), geoscience (Westoby et al. 2012), land cover studies (Clark & Hardegree 2005) and transportation (Jędrzychowski & Kujawski 2014) terrestrial monitoring has performed a very important role. Terrestrial monitoring of river ice is a cost effective and easy to use method of data acquisition (Bourgault 2008). River ice monitoring is often necessary to maintain navigation and for prediction and prevention of ice jams and floods. Shore-based terrestrial monitoring of river ice can be used

along with other *in situ* mounted instruments and remote sensing techniques for a better understanding of river ice processes.

A comprehensive research program has been conducted on Lower Nelson River (LNR), Manitoba- Canada since 2012, for a better understanding of river ice formation and break-up processes and its influence on river hydraulics. A 1,200-kHz Teledyne RD Instrument Acoustic Doppler Current Profiler (ADCP) and a 546-kHz shallow water ice profiling sonar (SWIPS) were deployed on a river bed under ice cover for measurements of stream wise velocity vertical profiles and ice cover conditions continuously during several winters (Ghareh Aghaji Zare et al., 2016a). The mounted instruments were accurate and reliable for measurement of the ice cover and river flow characteristics at single locations. However, in order to have a validation method for the measurements and also to obtain a spatial distribution of the ice cover, a monitoring technique based on terrestrial photogrammetry was developed. This paper provides a full description of the developed terrestrial photogrammetry technique and also the applied image analysis algorithm used for the assessment of the time series images taken at LNR.

The extracted results of this analysis are being used for calibration of ICESIMAT, a modified version of the ICESIM model, in MATLAB. ICESIM is a one dimensional river-ice process model originally developed by Acres International Limited (now Hatch) in 1973 for studies of the Nelson River hydroelectric plants (Zare, et al., 2015). For a better monitoring approach, two terrestrial cameras were mounted at two locations along the LNR. The field of view of each camera included the location of the bottom-mounted acoustic instruments used to measure and record hydraulic characteristics of the river during various ice cover processes. To develop the ultimate image analysis algorithm for terrestrial monitoring of river ice processes, several image analysis methods were utilized and some others were modified. This paper explains this

algorithm, which performs the initial pre-processing, geo-rectification, detection and calculation of the ice cover area and the border ice generation and recession, and extracts the results accordingly.

3.2. Investigation methods

3.2.1. Study Area

The Nelson River has a length of 2575 km and a drainage area of about 892300 km^2. This large river plays a very important role in the economy of the region as well as for Canada, both for its fish habitat and its series of hydroelectric generating stations. The study reach is the Lower Nelson River (LNR). LNR is considered as a regulated semi-alluvial river that drains Lake Winnipeg, to Hudson's Bay flowing in northern Manitoba, after spilling out into several other lakes (Newbury, 1986; Pip 1992). The study was conducted in a 102 km reach between Limestone Generating Station (LGS) and Gillam Island at the entrance of Hudson's Bay. This part of the river can be divided to two different sub-reaches based on the slope of the river bed. In the first 28 km, the slope of the river is about 0.0011 and a 30 m elevation drop occurs by several sets of rapids. The lower portion of the river has a milder slope of 0.00018. These two sub-reaches were selected for study of river ice cover processes (Figure 3-1).

Ice cover in the Lower Nelson River propagates by frazil generation during the exposure of surface water to super cold air, formation of floe ice sheets, and their downstream travel and accumulation where the flow rate decreases due to the mild slope near Gillam Island. Stable ice cover gradually propagates upstream from Gillam Island towards the LGS, usually in mid to late December, although there have been reports of ice front propagation as early as mid-November

and as late as mid-February (Acres, 2011). Topography and local hydraulic conditions such as steepness and water velocity have been reported as major factors controlling river ice cover thickening along the LNR (Ghareh Aghaji Zare et al. 2013).

The goal of the investigation was examine the effects of river ice cover processes on river hydraulics and sediment transport, thus two locations based on different flow characteristics were chosen for continuous data recording. These two locations were called “DX” and “Jackfish island” mounts, located within the high and low flow velocity sub-reaches of the LNR, respectively. The DX mount was located 35 km from LGS and 65 km from Gillam Island, in the steep bed section of the LNR. On the other hand, the “Jackfish Island” mount was located directly between LGS and Gillam Island.

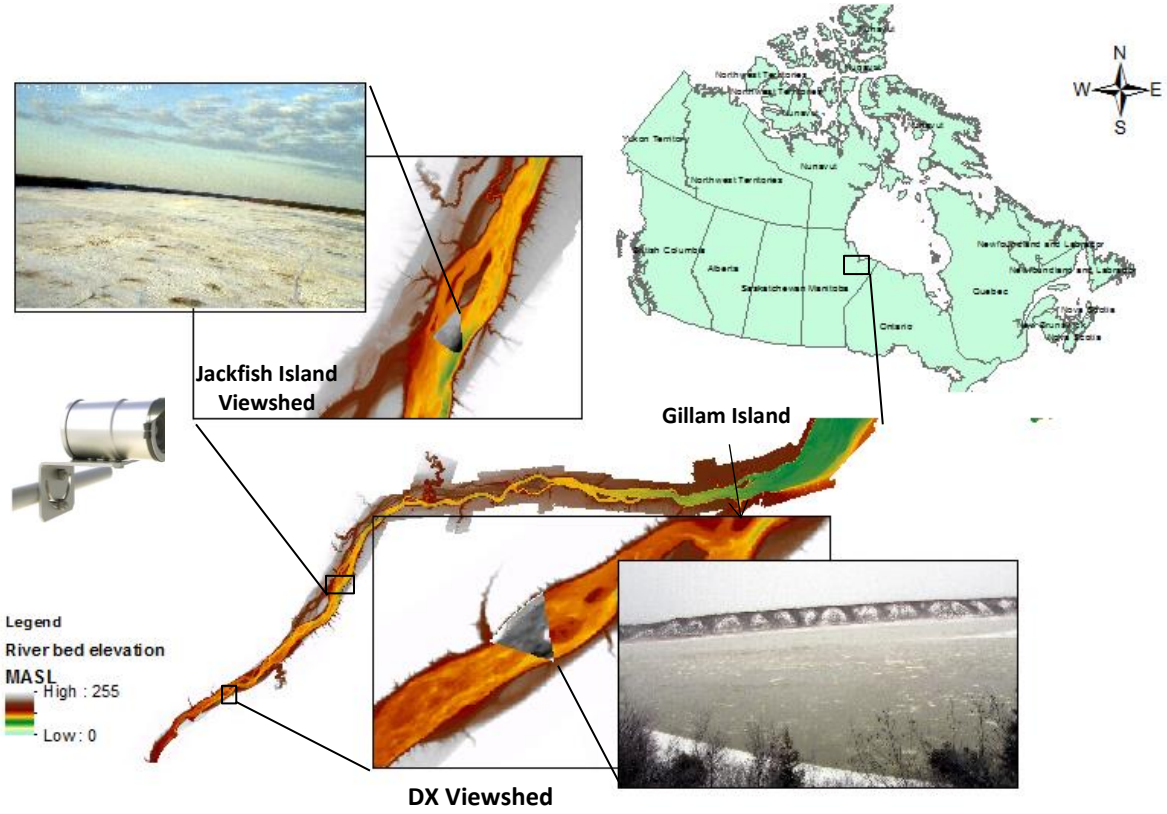

Figure 3-1. Study area locations and mounted camera along LNR; DX, and Jackfish Island (Respectively 65 and 50 km upstream of Gillam Island)

3.2.2. Field investigations, instrumentation and monitoring

Acoustic methods were employed in the research program for continuous hydraulic and sediment transport data collection. An ASL 546 kHz Multi-Functional Acoustic Water Column Profiler (MF- AWCP) along with a Teledyne RD Instruments 1200 kHz Sentinel Acoustic Doppler Current Profiler (ADCP) were deployed at both the "DX" and "Jackfish island" locations (Ghareh Aghaji Zare et al. 2014). A shore-based terrestrial camera was used at each location to monitor the ice cover processes, as a complement for the acoustic measurements. Figure 3-1 illustrates the deployment sites and mounted cameras. The mounting coordinates for both cameras at DX and Jackfish island were (457225.00 m E, 6286734.00 m N) and (469519.00 m E, 6299399.00 m N), respectively.

The deployment in "DX" location was performed on December 2012 for four months. Unfortunately the acoustic instrumentation deployed at this location could not be recovered, but the images taken by the camera that was mounted on a tree on the right bank of the river can still be used, and the results of this analysis are presented in this paper. The same analogous deployment was used to record river hydraulic data at the Jackfish Island site, where the slope of the river is mild, and the river flow velocity is lower. A camera was mounted on a tree on Jackfish Island, looking upstream, where data gathering was accomplished for three consecutive years. Time series images which have been analyzed for each mounting location are outlined in Table 3-1.

The cameras were Campbell Scientific CC5MPX digital cameras. This camera weighs 1.06 Kg, which is light enough for an easy mount and installation. The diameter of this camera is 9.3 cm and the length is 22 cm. The maximum programmable still image resolution of this model of

high-resolution digital camera in JPEG format is 2592×1944. Operating temperature of the camera is -40˚ to +60 ˚C and the built-in clock accuracy is ±2 min/year. This camera is also equipped with an optical zoom lens (4 to 12 mm) and its field of view is 27˚ to 80˚. The camera batteries were recharged on site using solar panels. Even so, based on daytime hours, camera battery life, and data storage, both cameras were programmed to take images with a 1280×720 pixels quality. The time lapse between images varied between time series. The time lapse for winter 2012-13 for both sites was 30 minutes; otherwise images were taken at Jackfish Island with a one hour time lapse.

Table 3-1 Number of terrestrial images taken at each of the mounting locations along the LNR

Site Name	DX Site		Jackfish Site	
2012-13	Dec- 2012	716	Dec- 2012	723
	Jan- 2013	752	Jan- 2013	992
	Feb- 2013	611	Feb- 2013	896
	March- 2013	197	March- 2013	215
	Total	2276	Total	2826
2013-14			Nov-2013	181
			Dec- 2013	497
			Jan- 2014	497
			Feb- 2014	425
			Total	1600
2015			Feb- 2015	308
			March- 2015	413
			April- 2015	498
			May- 2015	496
			June- 2015	27
			Total	1742

3.3. Image analysis algorithm

Due to the large numbers of images for each data set, an automated image analysis algorithm was developed to acquire accurate and reliable quantitative data from the time series images. The algorithm consists of four main discrete steps (subroutines) that collaboratively work to get to the final objective, i.e., automated time series image analysis for data extraction regarding ice cover

processes. As the first step, the algorithm initiates the preprocessing step and after accomplishment of the registration and rectification subroutines the algorithm finalizes the results using the target detection (ice) procedure. Final calculations are then performed to extract the quantity of the river ice cover area and border ice generation and recession rates, based on the detected and rectified pixels.

To the best of the authors' knowledge, only a few studies have previously reported shore-based terrestrial monitoring of river ice (Bourgault 2008; Jędrzychowski & Kujawski 2014). Notably none of these studies introduced an automatic algorithm for both rectification and detection purposes. Bourgault (2008) was able to successfully rectify oblique shore-based images of St. Lawrence River but did not introduce a method of automated river ice detection. Furthermore Ground Control Points (GCPs) played an important role in the rectification method. In the present study the rectification method of Corripio (2004); Härer et al. (2013) was modified for changing water surface. Also, unlike the other geo-rectification techniques applied in previous studies, the utilized geo-rectification technique in this study is not dependent on GCPs. This makes the technique suitable for remote places in which locating GCPs is a difficult and challenging task. Moreover the modification applied on the geo-rectification method makes this technique suitable for rivers with continuously changing water surface elevation.

Furthermore, a modified edge sensitive variational image thresholding technique (Ray & Saha 2006) for river ice cover detection and calculation was developed. The ice detection technique used in this algorithm was able to detect ice in the images taken with a camera without any filter. The detection subroutine employed in this algorithm is more accurate compared to similar studies (Jędrzychowski & Kujawski 2014). Finally, the presented algorithm was capable of extracting the quantity of river ice cover area, border ice generation and recession rate, which is a

unique achievement among similar studies. For the first time, the presented algorithm can perform a robust and automatic rectification, detection and calculation of river ice cover characteristics based on oblique terrestrial sets of images. This paper mainly focuses on the developed river ice monitoring and analysis algorithm as well as the acquired results.

3.3.1. Preprocessing

Image quality enhancement as well as reading and saving data recorded on each image are the two main tasks of the preprocessing step. Different weather conditions as well as sunlight were the two main factors that affected the quality and usability of the images. Precipitation and foggy weather could completely degrade the quality of the captured images. The main purpose of the preprocessing subroutine is to accelerate the image analysis procedure by either enhancement or elimination of the poor quality images. By upgrading the quality or removal of these images from the time series set, the algorithm could accomplish the processing and calculations more accurately and quickly.

Several methods of image quality assessment have been introduced. These methods can be classified as full-reference (FR) methods or no-reference (NR) methods. In FR, the quality of an image is assessed by comparison with the quality of a reference image (RI), while in NR the quality assessment is performed without any comparison with the original images (Thung & Raveendran 2009). Different image quality factors can be used for the assessment procedure, such as sharpness, noise, contrast, etc. Noise was the only quality factor used in this algorithm since a comprehensive image quality assessment did not seem to be necessary. Noise in images is a random brightness intensity or color distribution within the pixels of an image. Presence of fog and precipitation were the two main factors affecting the quality of images, and noise

removal in these images was performed using median filtering available in the Matlab image processing toolbox. Median filtering is one of the common image enhancement techniques. Unlike other linear methods, this technique is less sensitive to sudden extreme changes in pixel intensity, which is a prevalent issue in different parts of the images taken at LNR. Using the median filtering, salt and pepper noise of the images was removed successfully without reducing the sharpness of the images. As for the elimination of those images for which enhancement seemed to be impossible, average pixel intensity was used as a threshold of elimination.

The second part of the preprocessing step was reading and recording the air temperature as well as time and date, which were recorded on the upper section of the images. These data are vital for the analysis of the results, thus this step was added to the image processing algorithm.

3.3.2. Image registration

Camera movement due to wind was one of the challenging issues in image analysis and within the time series image sets. The movements can affect the rectification processes, leading to inaccuracies in final calculations, therefore this problem was also considered in the automated image analysis code before proceeding to the steps of rectification and detection. Using the Matlab image processing toolbox and an intensity and feature based solution for automatic registration, and with the application of the canny edge detection (Canny, 1986) and Hough transform concept (Hughes, 1990) all the images were registered to the reference image.

3.3.3. Rectification

A proper rectification is the most significant step in accurate quantitative data acquisition in photogrammetry. The large number of previous studies on geo-referencing and geo-rectification

methods is an indicator of the importance of this factor in the science of photogrammetry, especially in earth sciences (Corripio 2004; Bourgault 2008; Härer et al. 2013; Messerli & Grinsted 2015;) . Rectification was performed using the geo-referencing technique developed by Corripio (2004). This method involves the geo-referencing of oblique images to a digital elevation model (DEM) by defining a mathematical function to assign data of a DEM file to pixels of an image. This method is particularly useful for images with few or no Ground Control Points (GCP), as the method is mostly based on the internal and external characteristics of the camera (Härer et al. 2013). Several researchers have employed this method of rectification, mostly for snow cover pattern investigations (Schulz & De Jong, 2004; Durand, et al., 2005; Prokop, 2008). This rectification method has also been used in a computer model developed to monitor the snow cover pattern in mountainous areas (Härer et al. 2013).

Internal and external specifications of the camera are the main factors of the rectification algorithm based on this technique. Lens and image sensor dimensions, focal length, and also the image size are the internal specifications of the camera while the camera field of view (FOV), the position of the camera (latitude and longitude), its height, and the dip angle and the tilt angle around the axis are considered as the external characteristics of the camera that are used in the rectification process. This technique of rectification was particularly useful for this project, as it could be modified to deal with fluctuations in river water surface elevation between images. When a single image is geo-rectified with accurate reference data, then the pixels of that image are assigned to the rectified DEM coordinates. However, since the camera field of view is river water surface, increase and decrease of water level leads to up and down movements of ice in the images. In the case of water level increase, the upward movement of river ice cover may be detected as an increase in ice cover area. To solve this problem, the water surface elevation data

recorded with the pressure sensor on either the ADCP or an RBR sonde at the Jackfish Island bottom mounted instrument package were used in the modified rectification algorithm.

Reference images were chosen for each set of captured images at both sites, as the first step of the geo-rectification method. These images were in the same dimensions as other sets of time series images, with a high quality and captured on the same day that GCPs were recorded. (Figure 3-2) shows the reference image of Jackfish Island site on February 2015 with GCPs indicated as red dots; GCPs later were used to verify the geo-rectification step. Once the reference image was selected, a DEM raster file of the camera field of view was produced using ArcGIS 10.1, considering a 'virtual' camera on the river DEM raster file with the same camera specifications. Finally, based on the angular field of view of the camera, the imposition of the derived DEM layer on the reference image was performed. However, in order to rectify deficiencies due to changes of the water surface, prior to application of the Corripio et al. (2004) transformation technique, the elevation of the DEM layer was modified using the recorded LNR water surface elevation at Jackfish Island.

Figure 3-2 Reference image for the set of shore-based terrestrial images of 2015, red dots illustrate the Ground Control Points with their corresponding coordinates

The standard technique of perspective viewing presented by (Fiume, 1989 & Hughes, 1990) is the basis of the geo-referencing method. First, the points of the DEM file are mapped to the camera coordinate system. Second, a coordinate system is assigned to pixels of the image utilizing a specific transformation technique considering the viewing direction and focal length of the camera.

To transform the real coordinates to the camera coordinates the following transformation equation is used for a single DEM pixel:

$$\begin{pmatrix} P_{tx} \\ P_{ty} \\ P_{tz} \\ 1 \end{pmatrix} = \begin{pmatrix} 1 & 0 & 0 & -C_x \\ 0 & 1 & 0 & -C_y \\ 0 & 0 & 1 & -C_z \\ 0 & 0 & 0 & 1 \end{pmatrix} \begin{pmatrix} P_{wx} \\ P_{wy} \\ P_{wz} \\ 1 \end{pmatrix} \quad \textbf{[2]}$$

Where P_w is the location of a point in world coordinates system, and P_t is the translated point to a reference system with origin at the camera position, C.

After the translation of the world coordinates of the pixel point to the camera coordinates P_t, the translated coordinates should be rotated according to the viewing reference system. This reference system is defined using the viewing vector of the camera. Considering "T" as the target point of the camera, the hypothetical line connecting camera coordinates to "T", is called viewing vector, "N". Thus, the new camera coordinate system can be defined by, "N", "U", and "V", where "U" and "V" are the horizontal and vertical axis of the camera coordinate system.

Calculation of "N" based on the universal coordinates of the camera and its target point along with the calculations for "U" and "V", are presented in equations [3] to [6] (Corripio 2004):

$$\vec{N}_0 = T - C \quad \textbf{[3]}$$

$$\vec{N} = \frac{\vec{N}_0}{|\vec{N}_0|} \quad \textbf{[4]}$$

$$\vec{U} = \begin{cases} \vec{N} \times \dfrac{\vec{N}_{xy}}{|\vec{N}_{xy}|} & if \;\; N_z > 0 \\ \dfrac{\vec{N}_{xy}}{|\vec{N}_{xy}|} \times \vec{N} & if \;\; N_z < 0 \end{cases} \quad \textbf{[5]}$$

$$\vec{V} = \vec{N} \times \vec{U} \quad \textbf{[6]}$$

In the last two equations, $\vec{N}_{xy}$ is the projection of $\vec{N}$, on the horizontal plane. Defining the new camera reference system, the rotation process of the translated point P_t to camera reference system is performed using the following equation (Corripio 2004).

$$\begin{pmatrix} P_{cx} \\ P_{cy} \\ P_{cz} \\ \omega \end{pmatrix} = \begin{pmatrix} U_x & U_y & U_z & 0 \\ V_x & V_y & V_z & 0 \\ N_x & N_y & N_z & 0 \\ 0 & 0 & 1/f & 1 \end{pmatrix} \begin{pmatrix} P_{tx} \\ P_{ty} \\ P_{tz} \\ 1 \end{pmatrix} \quad \textbf{[7]}$$

In this equation, f is the focal length of the camera, P_c is the coordinates of a point in camera coordinates system, and ω is the scaling factor for perspective projection.

To correct for changing water surface, the target point elevation (T_z) is modified, leading to a change in the viewing vector elevation (N_z) in each image.

Once the DEM pixel point is translated to the camera coordinate system P_c (equation [7]), the final step is to perform the perspective projection, that is to scale P_c to the image panel. Following (Watt & Watt, 1992) and considering the image panel width, w this perspective projection is calculated as:

$$P_{px} = \frac{f P_{cx}}{\frac{1}{2} w P_{cx}} \qquad and \qquad P_{py} = \frac{f P_{cy}}{\frac{1}{2} w P_{cz}} \quad \textbf{[8]}$$

A georeferenced map is the output of the rectification subroutine for each image; this map is then imposed over the corresponding image. The superimposed DEM file on an image is utilized in river ice cover calculations after the target detection subroutine.

3.3.4. Target Detection

The final step of the image analysis algorithm, before the area calculations, is target detection; the main goal of this step is to detect automatically different kinds of river ice cover in available sets of geo-rectified images. Correct target detection is critical for accurate final results. Target detection in computer vision is performed using different techniques of image segmentation. In this research, target recognition of the river ice cover in the images was accomplished by utilizing "*thresholding",* the most common image segmentation method. In thresholding, an image is segmented into regions of interest, while all other sections of the image deemed inessential are removed (Wilson, et al., 2000).

In the thresholding technique of image segmentation, the RGB image is converted to gray scale and then, based on the intensity of the pixels and also a defined threshold, the gray scale image is transformed to a binary black and white image. In the binary image, white and black pixels respectively represent pixels with intensities higher or lower than the thresholding value. Automated river ice cover detection is not feasible without automatically defining the thresholding value. This is because the pictures at LNR were taken at different times of the day and in different weather conditions, thus the pixel intensities for ice and water were not consistent. Various pixel intensities for ice and water within the set of images, and even within a single image, make the segmentation procedure even more challenging (Figure 3-6).

Thresholding methods can be generally categorized as either global or local thresholding. In the global thresholding method the pixels of an image are compared to a single image intensity value, i.e., the global threshold. The most common global thresholding technique is a nonparametric and unsupervised automated threshold selection based on the gray level

histograms of an image (Otsu, 1975). This quick and easy thresholding method has previously been used successfully for image segmentation. However, this method of segmentation often fails if the illumination in an image varies spatially or temporally in a video stream (Bradley & Roth, 2007). As an alternative, in local image thresholding, dynamic selection of the thresholding value is performed locally based on the spatial variation in illumination. Several local image thresholding methods have been developed and tested for target detection (Niblack, 1985; Wellner, 1993; Liu & Luo, 2003; Yan & Hong, 2005; Bradley & Roth, 2007; Ray & Saha, 2007). In this paper, the edge sensitive variational image thresholding technique (Nilanjan & Saha, 2007), is modified to account for altering pixel intensities of ice and water in the time series of images.

The main goal of this subroutine is to find the optimized thresholding value, or function. When it comes to finding functions that are optimal based on some criteria the variational optimization concept is utilized. In calculus of variations, a "functional" is a function from the vector space to its corresponding scalar values, in other words it is a function that takes a vector and returns a scalar. In computer vision, the functionals that are used to quantify the quality of a particular solution consist of two major parts; one to measure the dependability of the solution to the observed data and the second to synthesize prior assumptions about the final expected solution (Treiber 2013).

In the employed method of thresholding, we used the variational energy functional proposed by Ray & Saha (2006). This variational energy functional consists of a non-linear combination of data and a regularization term. The utilized variational energy functional is a function of the threshold surface, the image, and a weighting parameter (Ray & Saha 2006) that balances the data and the regularization terms.

In this method, the image and the threshold are defined by functions as $I(x,y)$ and $T(x,y)$. Following Ray & Saha (2006), the proposed energy functional is:

$$E(T;\alpha) = \sqrt{1-\alpha^2}E_1(T) + \alpha E_2(T) \quad \textbf{[9]}$$

$$E_1(T) = 0.5 \iint g(x,y)\big(I(x,y) - T(x,y)\big)^2 dxdy \quad \textbf{[10]}$$

$$E_2(T) = 0.5 \iint |\nabla T(x,y)|^2 dxdy \quad \textbf{[11]}$$

$$g(x,y) = \frac{|\nabla I(x,y)|^q}{max(|\nabla \mathrm{I(x,y)}|^q)} \quad \textbf{[12]}$$

In these equations, the weighting parameter, α, is between 0 and 1. Since this method is based on the definition of an edge sensitive energy function, the first energy component in equation 9, E_1, is related to the edge indicator function g(x,y). The regularization term is E_2. Finally, the optimal threshold surface is found by an iterative minimax solution for the energy functional (Ray & Saha 2006). The optimal threshold surface finds a specific thresholding value locally and for each image, which leads to a more accurate segmentation procedure.

Due to the sunshine and precipitation at different times of the day, pixel intensities of visible ice cover patches vary between images and within a single image. Application of the edge sensitive variational image thresholding method led to improved image segmentation in the available time series images. Ice detection using this method led to proper ice and water detection. However, some inconsistencies in the detected images were recognized for images of the times series captured at different times of the day. The employed image segmentation method was also incapable of completely acceptable river ice detection for images taken in severe reflectance of

sunshine. In order to solve these issues and to enhance the application of the detection subroutine, an extension to the thresholding algorithm was added. Specifically, severe sunshine glare and its reflectance on the water surface were eliminated with an added extension within the ice detection algorithm which masks both the sunshine and its reflectance in the images. This mask was produced using global thresholding for the sunshine glare pixel intensities. In addition, in order to improve consistency of the river ice detection procedure, the images of the time series were automatically categorized based on date and time of the day prior to the application of the above mentioned edge sensitive variational image thresholding technique. In this technique, images are categorized before segmentation, such that ice can be classified as either brighter or darker (above or below the thresholding surface) than water for that particular section of that particular image (Figure 3-3). Based on this categorization, thresholding technique is performed separately for different sections of the image for images with wide range of pixel intensity.

Ultimately, the image analysis algorithm drew boundaries around the detected river ice patches in each image. The traced boundaries and their corresponding pixel coordinates were then converted to the real world coordinates based on the superimposed DEM layer on each image, and the rectified pixels. Further calculations such as river ice cover area and border ice growth and recession were also accomplished based on the detected rectified pixels of ice and water. Along with the recorded time and air temperature associated with each image, these results were used to assess full ice cover formation and break-up patterns. Figure 3-3 indicates the working steps of the developed image processing algorithm, in a flow chart.

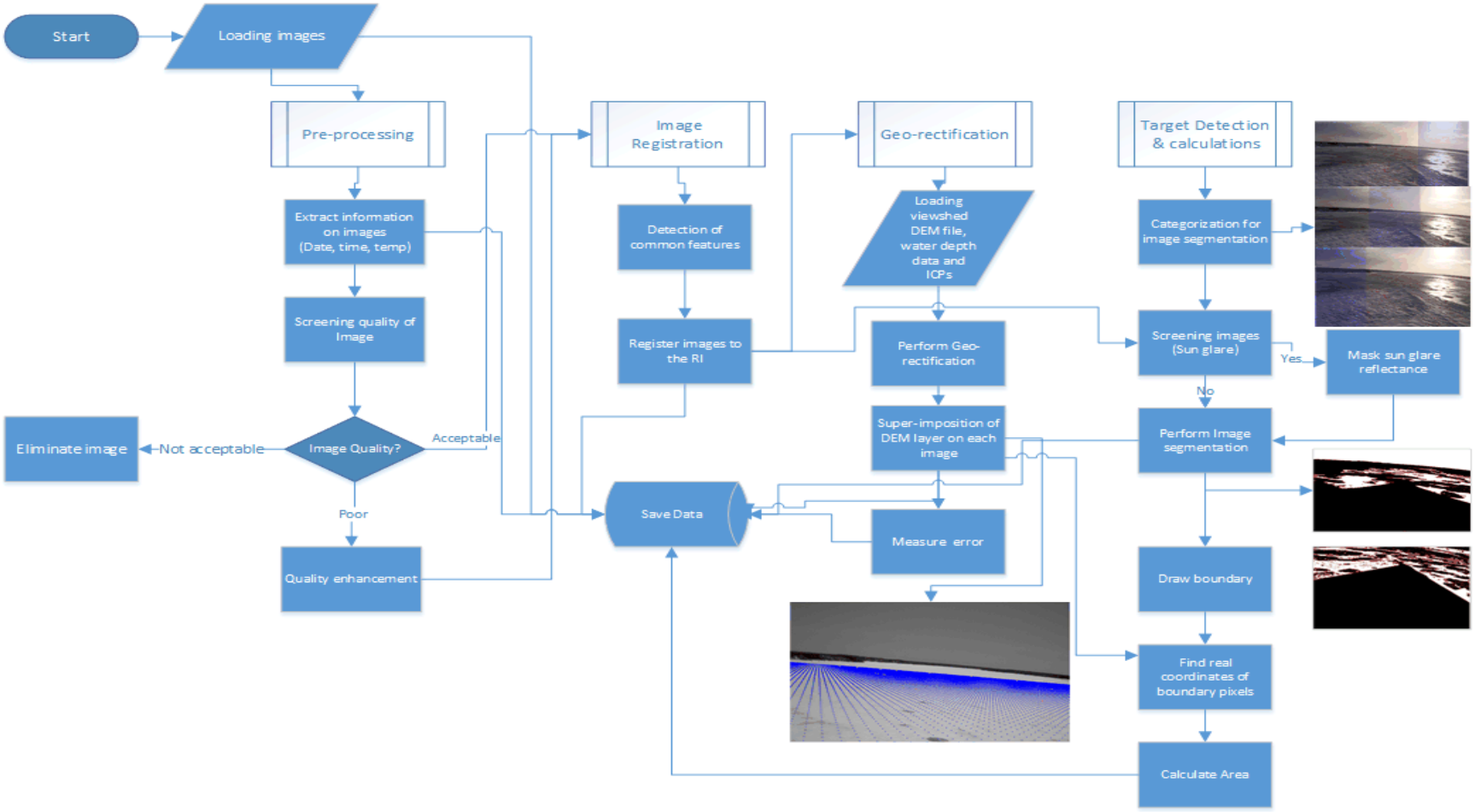

Figure 3-3 Steps of the developed image processing algorithm shown in a flow chart

3.4. Results and Discussion

3.4.1. Verification of the algorithm

Validity of the two major subroutines of the algorithm, *geo-rectification* and *target detection,* were evaluated independently. The rectification method was verified using Ground Control Points (GCPs) obtained during the stable ice cover period. The GCPs were helicopter positions on the river ice surface recorded with a GPS. Figure 3-2 shows the reference image with the recorded GCPs for winter 2015 at the Jackfish Island location. The average distance root mean square error (RMSE) of the rectified reference images was less than 30 meters which was considered acceptable for rectification of the terrestrial images of this project.

Verification of the *target detection* step was performed by manual detection of the river ice cover boundaries. The manual detected ice cover boundary pixels are then used for area calculation based on the corresponding real world coordinates. Four sample images from the Jackfish Island and DX sites, representative of the entire time-series of available images, were used for this purpose (Table 3-2). The first two images were taken at Jackfish Island in November 2013. The triangular shaped ice in the near-field close to the camera is the border ice formed on the margin of the island, which grew gradually in the images of the subsequent months. Pictures number 3 and 4 of Table 2 were taken at the DX site in January and February 2013, respectively. Picture number 3 shows automatically detected ice floes with an area of about 7568 m^2. On the other hand, in picture number 4 a 1300 m^2 open water patch was detected.

The overall total RMSE error of ice area detection for the developed image analysis algorithm including the image rectification and target detection subroutines were calculated using the following equation:

$$Total_{Error} = \sqrt{(geo\ rectification_{Error})^2 + (target\ detection_{Error})^2} \quad \textbf{[13]}$$

The total RMSE error in the analyzed images ranged from 50 m^2 to 253 m^2.

Table 3-2 Sample analyzed images taken at Jackfish Island and DX sites

No	Original Image	Analyzed image	Image location	Automated calculated river ice area [m2]	Manually calculated river ice area [m2]	RMSE [m2]
1		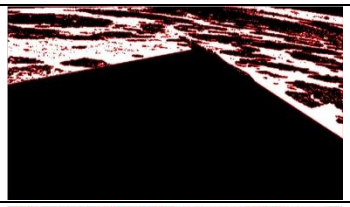	Jackfish Island	485717	486103	248
2	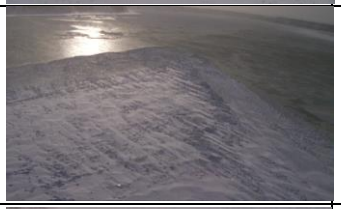	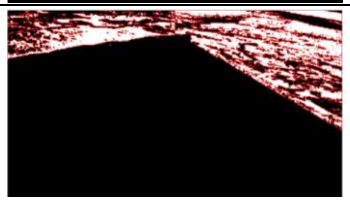	Jackfish Island	485289	485310	156
3		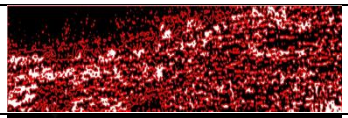	DX	7568	77883	253
4		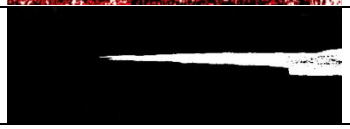	DX	1300	84152	50

3.4.2. Ice regimes along the Nelson River

River ice cover formation in LNR initiates by frazil ice generation during freeze-up. Figure 3-4 shows the time series of average daily air temperatures during the 2012-13 winter. Air temperature at LNR was consistently below 0^{o} C after late October, when frazil ice generation initiated along the river. The generated frazil ice ultimately floats to the surface of the water, aggregating into ice floes. Figure 3-5 shows the river ice condition at the DX location in October 2012 when the floating ice floes were travelling downstream. Discharge data at Jackfish Island and DX locations were calculated based on the time shifting of recorded discharge at LNR. Weekly moving average discharge and water depth fluctuations at Jackfish Island along the LNR (Figure 3-6) indicate that there was an increase of water depth during the period of decreasing discharge. River ice conditions on 11/Jan/2013 at both the Jackfish Island and DX locations are shown in Figure 3-7, when at the upstream DX location the ice floes were flowing downstream, while at Jackfish Island a partially stable ice cover had formed. The reason for this is the slope of the river bed which is steeper at DX location compared to Jackfish Island, and also the upstream progression of ice front from downstream towards upstream which had not occurred yet. In the following, results of the image analysis algorithm for the available time series images at the DX and Jackfish Island locations are presented in separate sections.

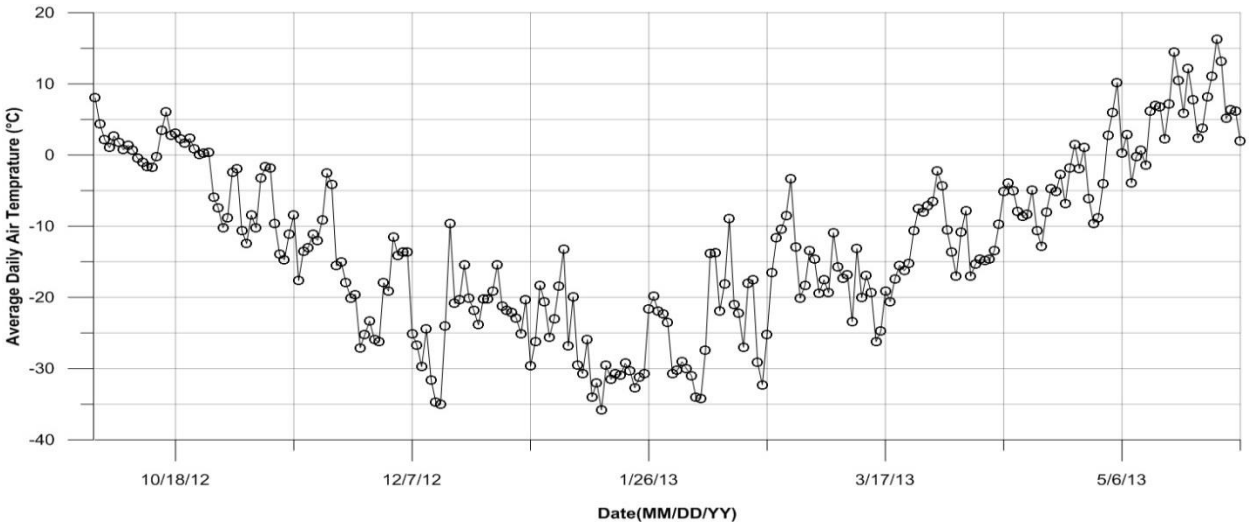

Figure 3-4 Time series of average daily air temperatures during winter 2012-13 recorded at Gillam, Manitoba (source: Environment Canada-Gillam Station)

Figure 3-5 River ice condition at DX location along the LNR on the second week of October, the generated ice floes are traveling downstream of the river

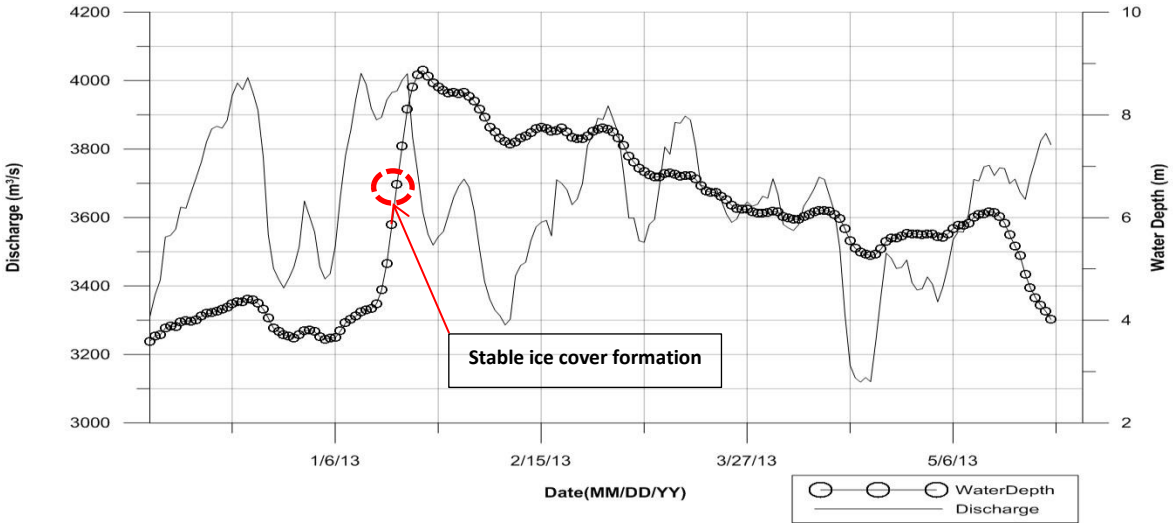

Figure 3-6 Weekly moving average discharge and water depth at Jackfish Island location for 2012-13 winter (Source: Manitoba Hydro)

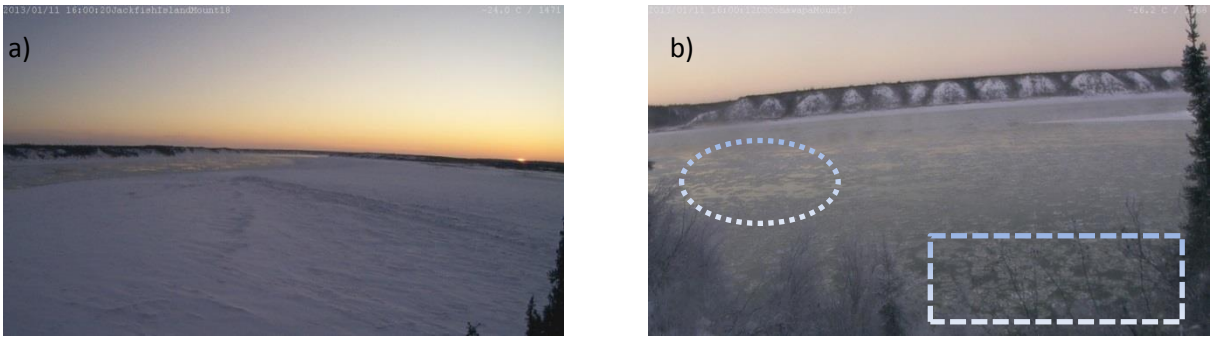

Figure 3-7 River ice conditions at two locations along the LNR on 11/Jan/2013. a) Jackfish Island location b) DX location; ice in oval has relatively darker pixel intensity; ice in rectangle has relatively brighter pixel intensity

DX site was chosen to mount the measurement equipment to investigate the influence of river ice cover on river hydraulics in a location with higher water velocity due to the steepness of the river bed. The monitoring camera at this location was mounted on a tree trunk at the right bank of the river looking to the left bank. The viewshed of this camera is shown in Figure 3-1. The camera was programmed to take pictures every 30 minutes during daylight. Monitoring started on

December 2012 to March 2013 and around 2300 images were taken over this period. The georeferencing process was performed using the total viewshed of the camera at DX location, shown in Figure 3-1. However, due to the low visibility of river ice in the images and to lessen the errors in detection step, an area of about 85500 m^2 was cropped for processing. Figure 3-8 illustrates the average daily time series of recorded air temperatures at DX location using the camera built-in thermometer, water discharge and the calculated area covered by ice as a percentage of the processed camera viewshed area.

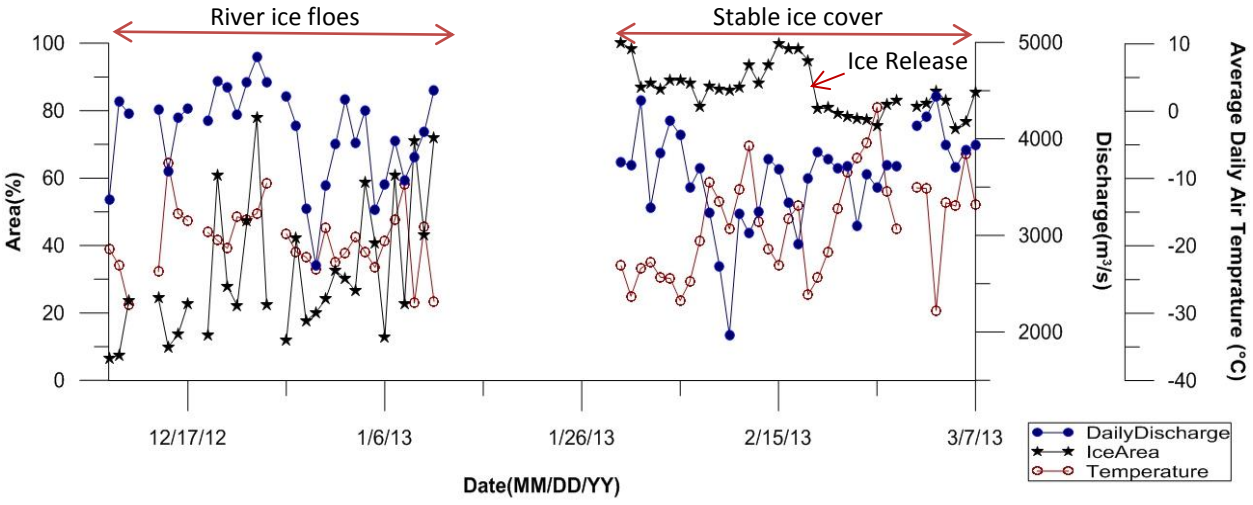

Figure 3-8 Extracted river ice cover area, water discharge and average daily air temperature at DX location along LNR for the duration of December 2012 to March 2013

Temperature at the DX location was consistently below zero for the entire duration of the monitoring period (Figure 3-8). Time series images show that at the beginning of winter (December 2012 to January 11, 2013) ice floes existed and there was no stable ice cover. Consequently, in this period variation in ice cover area was related to the density of ice floes travelling through the DX site. However, stable ice cover was established by January 30, 2013, when the entire investigated area of 85500 m^2 was detected to be covered by ice. Unfortunately,

in the period of stable ice cover formation, which happened during the second and third weeks of January 2013, some images were lost due to snow stuck on the camera lens. However, the sudden increase of water level (25th January 2013), shown in Figure 3-6, is an indication of stable ice cover formation. The stable ice cover formed at the DX location did not last long, as on the next day an open water patch with an area of about 1330 m^2 started growing. This open water patch, which was formed due to the high velocity of flow at the location, existed for the entire duration of the available images.

A partial harmony between river ice cover area and daily river discharge graphs can be recognized in Figure 3-8. This graph can be divided to two different sections. The first section is when no stable ice cover was detected and river ice floes were travelling downstream of DX location. In this section increase and decrease of river ice cover area, which is the area related to ice floes, have a direct relationship with the fluctuations of river discharge. The second section of the graph represents the stable ice cover period, when the fluctuations of the river ice cover area were due to the growth and shrinkage of the open water patch area. Smoothness of the ice and continuous formation and ablation of the open water patch indicates thermal growth and shrinkage of ice cover in the patch. This is likely related to the thermal budget. However, defining a fixed pattern for open water patch growth and shrinkage in relation with air temperature and water discharge is complicated. The observations suggest that changes in discharge affected the open water patch area in different ways. Increase in discharge led to increase of thermal ice growth, and shrinkage of the open patch (see Figure 3-8, 13-15/02/2013). This is likely related to the thermal budget, wherein increased discharge leads to increased water velocity and consequently a decrease in thermal budget which facilitates the formation of ice cover in the open water patch.

On the other hand, increase in water discharge could also lead to river ice cover decrease due to growth of the open water patch (see Figure 3-8, duration of 31/01 to 01/02/2013). This phenomenon occurred in short time periods, when increase in water discharge led to increase of water surface elevation which in some cases led to the fracture of thin layer and growth of the open water patch. This was often followed by the formation of a complete layer of thin thermal ice.

A major detachment and release of river ice cover and its travel out of the viewshed of the camera occurred at 3 pm February 18th 2013, when the open water patch area doubled in just two hours. Figure 3-9 shows a two day hourly time series of the river ice cover, water discharge and air temperature related to this detachment process. The detachment process occurred during hydropeaking. Water discharge rose from 3439 m^3/s at 7:00 am to 4329 m^3/s at 11:00 am, which is a sudden increase of water discharge in just 3 hours, and then subsequently decreased to 2870 m^3/s at 15:00 pm. This sudden increase and decrease in water discharge led to increase and decrease in water surface elevation. Sudden fluctuations of water surface elevation led to a big crack along the weaker section of the river ice and ultimately its detachment and advection downstream.

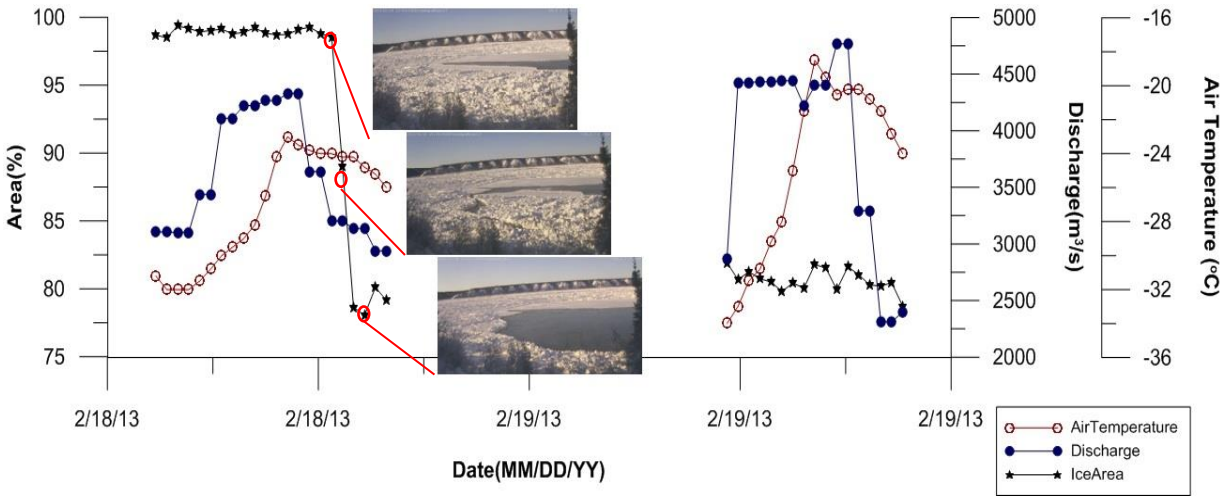

Figure 3-9 Two day hourly river ice cover area, water discharge and air temperature for the duration of February 18th to 19th 2013

3.4.3. Jackfish Island site

The Jackfish Island monitoring location was chosen due to its relatively mild slope, which allowed for comprehensive study of the effects of river ice cover on sediment transport. Unlike the mounted equipment of DX location, the measurement equipment on Jackfish Island site were successfully mounted and retrieved for three years of study; hence images were obtained during the three winters of 2012 to 2015. While border ice growth and open water patch were monitored the first two winters, in winter 2015 stable ice cover break-up was the aim of the monitoring. The total monitoring area in the time series images was around 492408 m^2 and results are presented as a percentage of this area. Average daily air temperature, river water discharge and area covered by ice and water for the duration of December 2012 to May 2013 are shown in Figure 3-10. Air temperature for the duration of the investigations was below -15^o C and a partially stable ice cover was detected to cover almost the entire 1 km width of the river except an open water patch on the right bank of the river. Ice sheets were also detected in the open water patch flowing

to the downstream. Figure 3-11 shows a sample Jackfish Island image from 2012 along with an aerial picture of the open water patch at the location. The time series of the images show that this open water patch was covered with stable ice by late January 2013, 5 days prior to the stable ice cover formation at DX location.

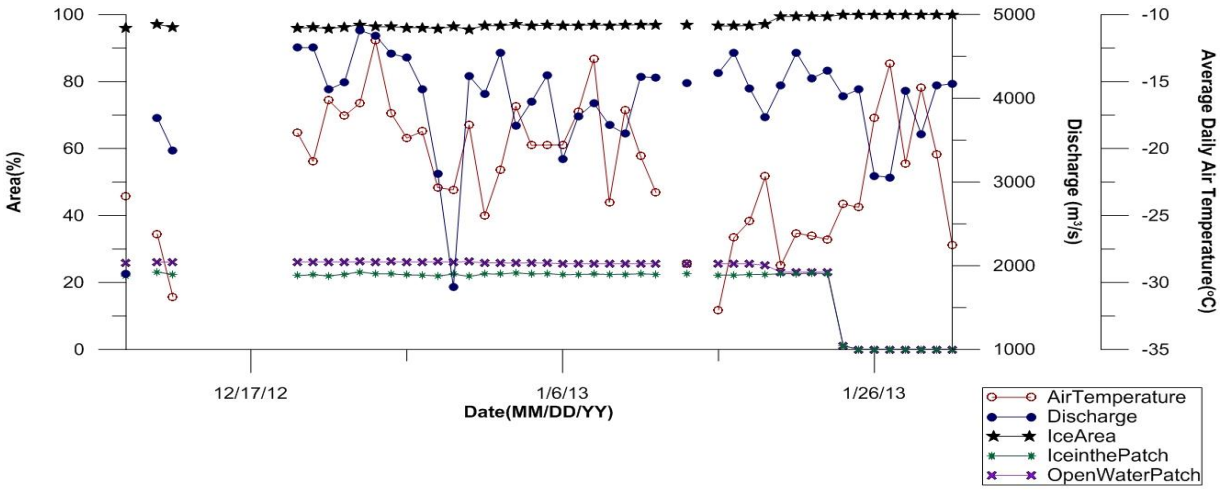

Figure 3-10 River ice cover area, river discharge and air temperature extracted from the time series terrestrial images at Jackfish Island location along LNR for the duration of December 2012 to February 2013

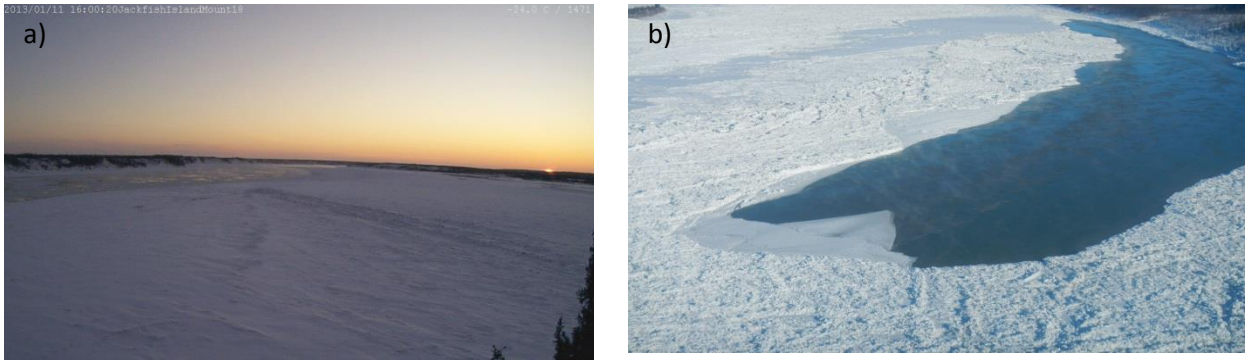

Figure 3-11 River ice cover conditions at Jackfish Island location along LNR for the duration of December 2012 to February 2013 a) Sample image of the time series set b) Areal image

Unlike the images of DX location, the open water patch at Jackfish Island location is not clearly visible due to its distance from the monitoring camera; however the reflectance of sunlight especially on images taken at sunrise and sunset helped in obtaining reasonable results.

Second winter terrestrial monitoring of river ice at the Jackfish Island site started in the third week of November 2013 and continued until the end of February 2014. Figure 3-12 shows the average daily air temperature, river ice cover and open water area along with river discharge. A triangle shape border ice that formed on the margins of Jackfish Island is visible in the time series images of this winter (Figure 3-13-a). Jackfish Island border ice increased gradually while air temperature decreased in November to December 2013 (Figure 3-13-b&c). The growing border ice ultimately connected to the other growing ice cover sections (Figure 3-13-b&c) and formed a stable ice cover (Figure 3-13-d). Figure 3-12 indicates that border ice grew gradually as the temperature dropped, and sudden temporary increases of temperature did not stall border ice growth. However, a sudden drop of river ice cover area was detected on Dec 1st 2013 which was due to the decrease in river ice floes. Total ice cover area data shown in Figure 3-12 is the summation of the areas related to border ice and ice floes.

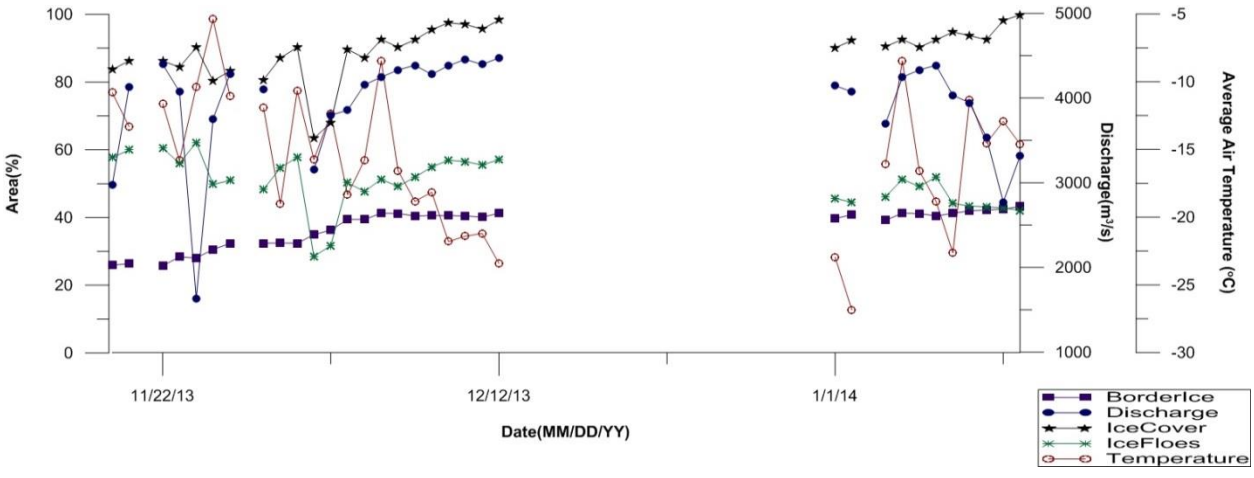

Figure 3-12 River ice cover area, water discharge and air temperature extracted from the time series terrestrial images at Jackfish Island location along LNR for the duration of November 2013 to February 2014

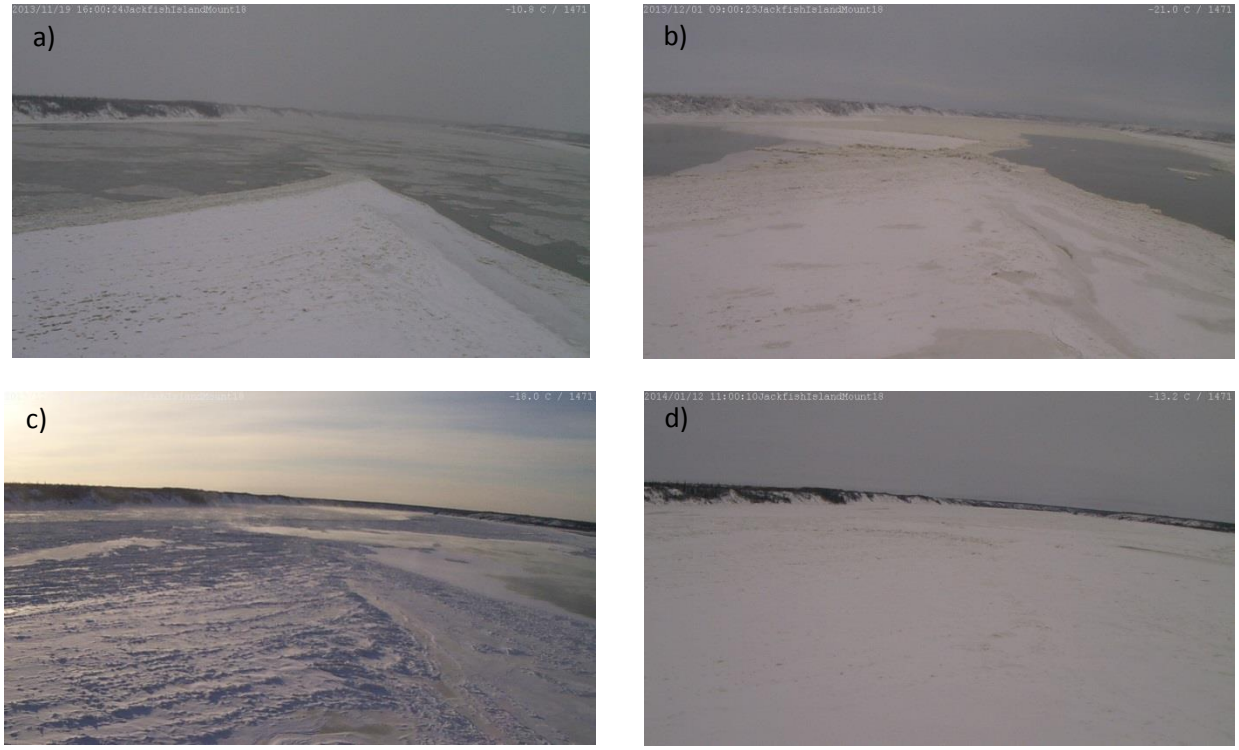

Figure 3-13 River ice conditions at Jackfish Island along the LNR for the duration of November 2013 to February 2014; a) 19/Nov/2013 b) 01/Dec/2013 c) 01/Jan/2014 d) 12/Jan/2014

Investigations during the third winter started on February 9th and continued until June 2nd 2015, focusing mainly on the break-up period. As the stable ice cover formed sometime before monitoring, the time series images showed stable firm ice cover during the period of February 9th to April 24th, at which the stable ice cover started to get thinner due to air temperature increase in the prior week. Figure 3-14 illustrates the river ice cover, water discharge and daily average air temperature at Jackfish Island from the beginning of ice cover thinning (April 24th) to the occurrence of break-up (25th May). The ice cover softened and thinned for an entire month of positive air temperatures and discharge fluctuations before breaking up. Figure 3-15-a shows the river ice cover condition at Jackfish Island on April 24th when the darker sections on river ice cover indicate melted water on the ice cover. Surface melting of the river ice was detected to

continue during the subsequent week of relatively warm air temperature. Figure 3-15-b shows the river ice condition and the melted water on the ice on May 2nd, 2015. Subsequently, air temperature dropped suddenly from 20 ^{0}C to near zero, and melted water on the ice froze overnight such that river ice covered the total monitored area of 492408 m^2 (Figure 3-15-c). Despite subsequent increased air temperature, stable river ice cover remained for another two weeks until May 18th when the last melting procedure that led to the ultimate break-up commenced.

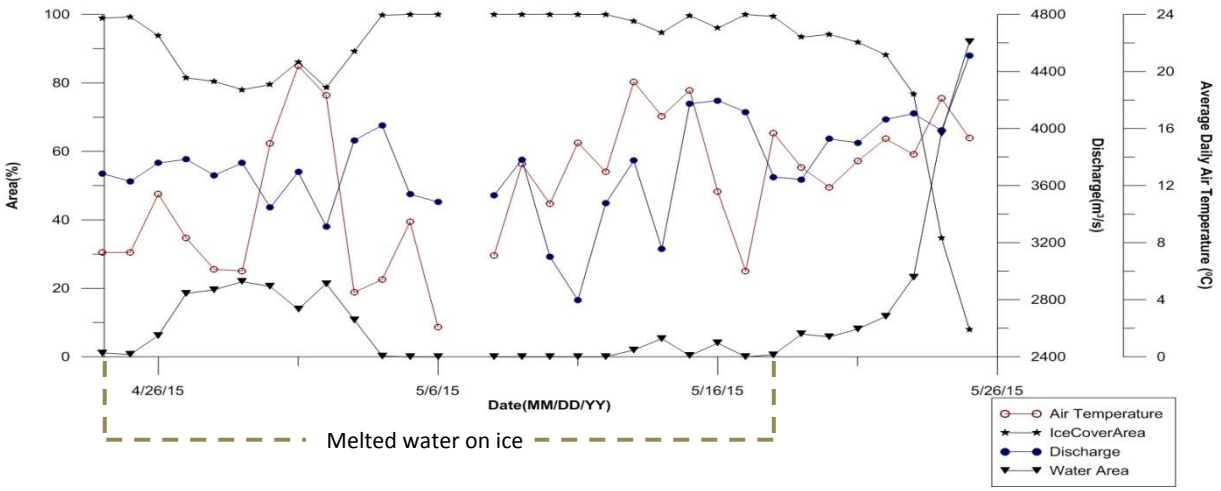

Figure 3-14 River ice cover area, water discharge and air temperature extracted from the time series terrestrial images at Jackfish Island location along LNR for the duration of April 2015 to May 2015

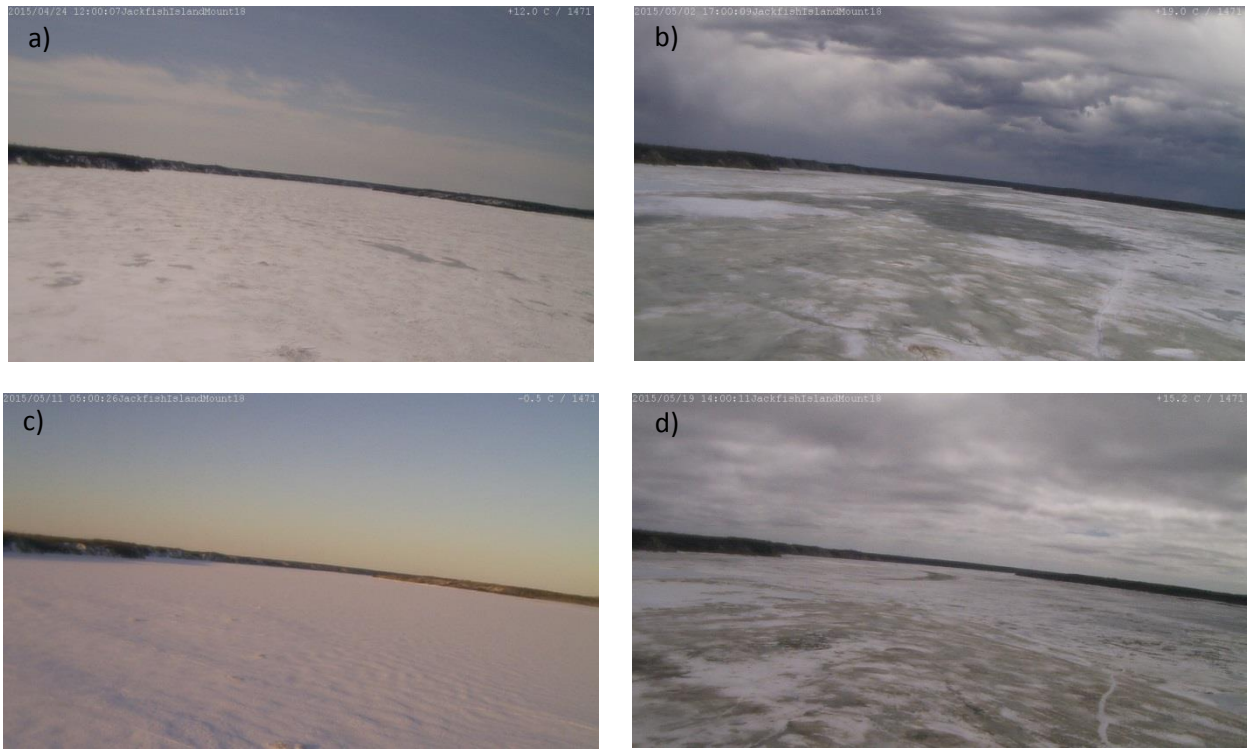

Figure 3-15 River ice cover condition at Jackfish Island site along the LNR, a) April 24th, detected melted water on ice b) May 2nd, increased melted water on ice, c) May 11th, frozen melted water on stable river ice with a snow cover d) May 19th, river ice cover detected to start melting

The ablation and decay of river ice cover continued until the final break-up and removal which occurred in over two days from 22nd to 24th of May, following an increase in river discharge. Figure 3-16 shows the sequence of river ice cover conditions during break-up. Hourly data of river ice cover area along with air temperature and river discharge for this three day period are shown in Figure 3-17. At the beginning of this period the river ice cover was thin due to thermal weakening (Figure 3-16-a). Increase in water discharge and hydro peaking assisted the mechanical ablation and removal of river ice cover. On May 22nd an area of about 53000 m^2, greater than 10% of the visible river surface, was detached and removed (Figure 3-16-b). An overnight rapid decrease of air temperature and river discharge led to the re-formation of the river ice cover by 4:00 am on May 23 (Figure 3-16-c). The newly formed river ice cover did not last long and by the afternoon of the same day the ultimate removal of river ice cover occurred

(Figure 3-16 d, e & f). Figure 17 indicates that both the initial and final removal of the ice cover occurred during flow augmentation due to hydro-peaking.

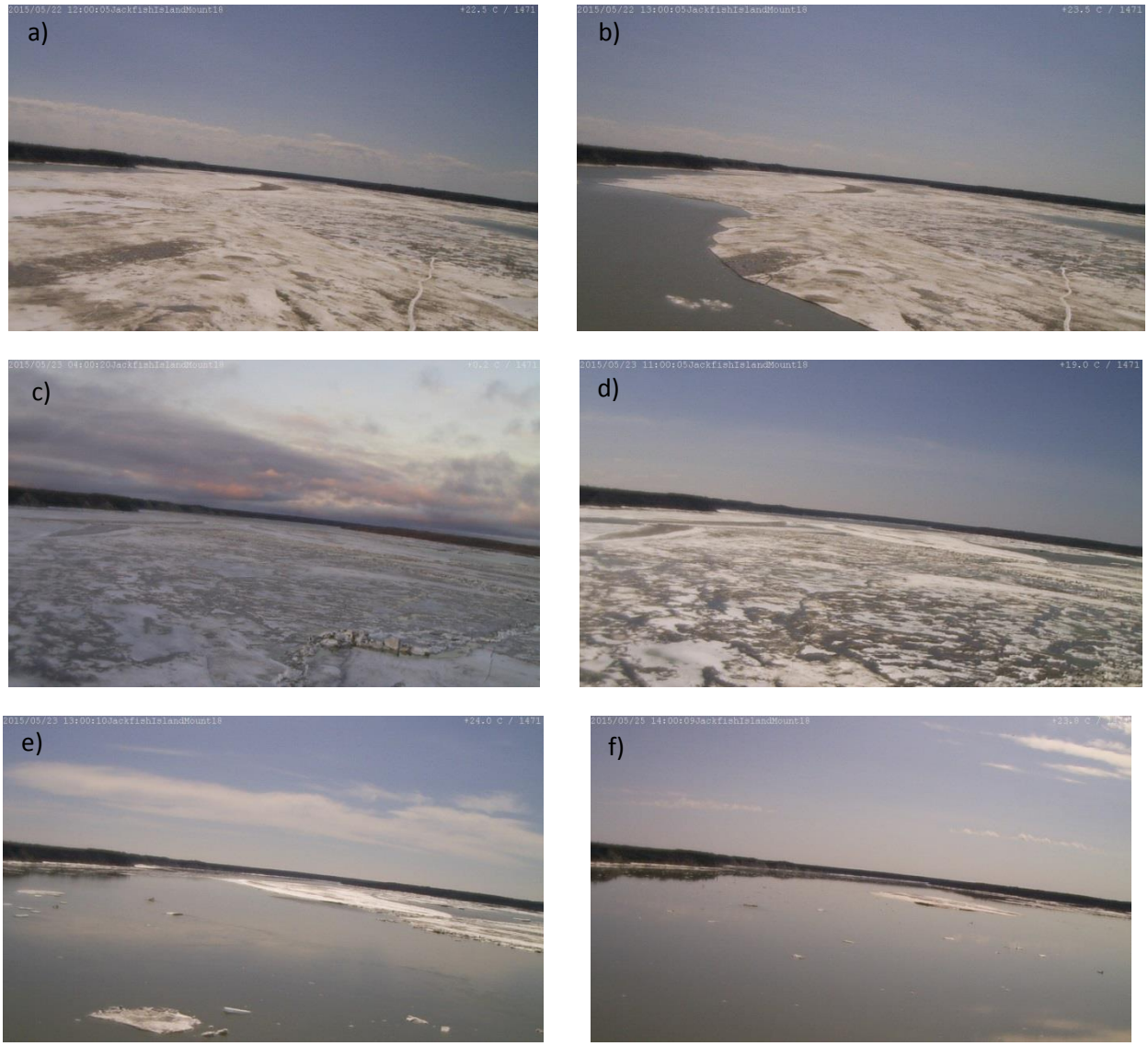

Figure 3-16 River ice cover conditions at Jackfish Island along LNR, a) May 22nd at 12:00 pm, river ice cover decay b) May 22nd at 01:00 pm, removal of a considerable part of river ice cover c) May 23rd at 04:00 am, partially complete river ice cover is detected d) May 23rd at 11:00 am, thin river ice cover is detected e and f) May 23rd 01:00 to 2:00 pm, complete removal of river ice cover, flowing ice pans are detected

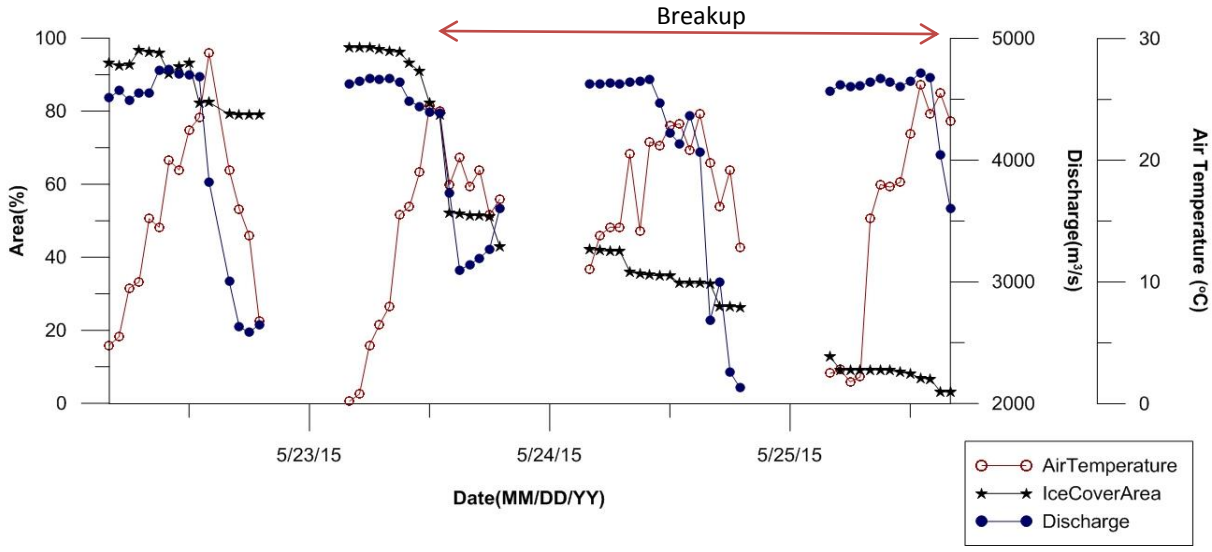

Figure 3-17 Three day hourly extracted river ice cover water discharge and air temperature at Jackfish Island location along LNR for the duration of May 22nd to May 25th

3.5. Conclusion

Several image analysis techniques were modified and employed to develop a river ice cover shore-based image analysis algorithm. This algorithm consists of four major subroutines, including “preprocessing”, “image registration”, “geo-rectification” and “target detection”. The first two subroutines of the algorithm were added for preparation of the images for processing. The issues regarding the quality of the images were solved in preprocessing step. Image registration subroutine was also added to solve the issues regarding the movements of the camera. In this step all the images were assigned to the reference image before proceeding to georectification and target detection step. Superimposition of a DEM map of the camera FOV on an image using camera intrinsic and extrinsic characteristics was utilized to assign correct coordinates of pixels of an image. In the fourth subroutine of the algorithm, locally adaptive image thresholding was implemented to detect river ice. Unique approaches were applied in the geo-rectification and target detection steps to overcome challenges such as surface elevation

fluctuations and variation in pixel intensity. The developed algorithm provides objective quantification of river ice cover from oblique shore-based images. Different river ice cover characteristics such as area covered by ice, open water patch generation and ablation, border ice growth rate, and the location of the leading edge were detected and quantified using this algorithm. Results show that thermal budget plays a very important role in growth and ablation of river ice cover. Increase in water discharge rate that leads to water surface elevation increase also affects river ice processes by inducing, mechanical detachment of river ice cover specifically in thin and weaker sections. The quantitative observations obtained in this study can potentially be used to improve river ice formation and break-up algorithms.

The advantage of providing quantitative and objective information of the presented technique makes this algorithm a suitable tool for automated analysis of shore-based terrestrial imagery; and it is suitable to be employed in various river and environmental researches as well as maritime transportation. Application of the lens filters is recommended for quality enhancement of the images which leads to better and more accurate data extraction. It is also recommended to use more than one camera covering whole target area for accurate monitoring of further distances.

Chapter 4

Conclusions and recommendations

An automated shore-based image analysis algorithm was developed in this thesis for river ice monitoring of Lower Nelson river. Several image processing techniques were implemented in four main subroutines of this algorithm. The four subroutines of the automated image analysis algorithm include “preprocessing”, “image registration”, “geo-rectification” and “target detection”. The developed algorithm has the following features:

- It allows for image quality enhancement, noise removal and automatic elimination of poor quality images.
- Image registration was used to rectify wind induced camera movements. Registration of the images to a reference image of the time series facilitates an accurate georectification process.
- Novel approaches were employed in the georectification subroutine to overcome the challenges induced by the fluctuating river water surface.
- A locally adaptive image thresholding technique was employed for image segmentation.
- River ice detection challenges induced by various pixel intensity patterns in the time series of the images were successfully overcome by utilizing a categorization algorithm of the time series images.

Some important conclusions were also reached after a quick analysis of the algorithm outputs:
As the main conclusion the developed method was able to detect and quantify vital river ice

cover characteristics, such as the area covered by ice, open water patch generation and ablation, border ice growth rate, and the location of the leading edge. It was also found that:

- The thermal budget of river water plays an important role in thermal river ice growth.
- The increase in surface water elevation which is induced by river discharge caused mechanical detachment of the river ice cover.
- The monitoring of river ice during break-up indicates that, the break-up procedure began with initial thinning and smoothing of both the surface and underneath of the river ice once weakened. Full break-up occurred in a very short period of time, during a period of increasing discharge.

In conclusion, the presented automated image analysis algorithm proved to be a useful tool for shore-based terrestrial monitoring, able to provide accurate, objective and quantitative information about the ice cover. We believe this method can be useful if employed in similar shore-based river water monitoring studies. We also believe that the use of more than one camera located along the length of the field of view will lead to more accurate monitoring of farther areas. If feasible, it is also recommended to use lens filters to reduce sun glare, and to minimize the effects of atmospheric haze, moisture, and other pollutants which lead to image quality degradation. Lastly, multi-spectral imaging may provide further information about ice cover in future deployments.

References

Ashton, G.D., 1978. River ice. *Ann. Rev. Fluid mechanics*, 10, pp.369–392.

Barker, R., Dixon, L. & Hooke, J., 1997. Use of terrestrial photogrammetry for monitoring and measuring bank erosion. *Earth Surface Processes and Landforms*, 22(13), pp.1217–1227.

Beamish, A.L. et al., 2016. Phenology and vegetation change measurements from true colour digital photography in high Arctic tundra. *NRC Research Press*, 49(May), pp.33–49.

Beltaos, B.S., 1984. River Ice Jams : Theory , Case Studies , and Applications. , 109(10), pp.1338–1359.

Beltaos, S., 2011. Developing winter flow rating relationships using slope-area hydraulics. *River research and applications*, 22(June 2010), pp.1085–1095. Available at: http://doi.wiley.com/10.1002/rra.1112\npapers2://publication/doi/10.1002/rra.1112.

Beltaos, S., 2016. Extreme sediment pulses during ice breakup, Saint John River, Canada. *Cold Regions Science and Technology*, 128, pp.38–46. Available at: http://linkinghub.elsevier.com/retrieve/pii/S0165232X16300891.

Beltaos, S., 2001. Hydraulic Roughness of Breakup Ice Jams. , 127(August), pp.650–656.

Beltaos, S. & Burrell, B.C., 2016. Transport of suspended sediment during the breakup of the ice cover, Saint John River, Canada. *Cold Regions Science and Technology*, 129, pp.1–13. Available at: http://linkinghub.elsevier.com/retrieve/pii/S0165232X1630088X.

Best, H., McNamara, J.P. & Liberty, L., 2005. Association of Ice and River Channel Morphology Determined Using Ground-penetrating Radar in the Kuparuk River, Alaska. *Arctic, Antarctic, and Alpine Research*, 37(2), pp.157–162.

Bourgault, D., 2008. Shore-based photogrammetry of river ice. *Canadian Journal of Civil Engineering*, 35, pp.80–86.

Calkins, D.L., Deck, D.S. & Martinson, C.R., 1982. Resistance coefficients from velocity profiles in ice-covered shallow streams. *Canadian Journal of Civil Engineering*, 9, pp.236–247.

Canny, J., 1986. A computational approach to edge detection. *IEEE transactions on pattern analysis and machine intelligence*, 8(6), pp.679–698.

Clark, P.E. & Hardegree, S.P., 2005. Quantifying Vegetation by Point Sampling Langdscape Photography Time Series. *Rangeland Ecology & Management*, 58(6), pp.588–597.

Corripio, J.G. et al., 2004. Land-based remote sensing of snow for the validation of a snow transport model. *Cold Regions Science and Technology*, 39(2-3), pp.93–104.

Corripio, J.G., 2004. Snow surface albedo estimation using terrestrial photography. *International Journal of Remote Sensing*, 25(24), pp.5705–5729.

Das, A. et al., 2015. Monitoring the freeze-up and ice cover progression of the Slave River 1. , 621(January), pp.609–621.

Ettema, R. & Zabilansky, L., 2004. Ice Influences on Channel Stability: Insights from Missouri's Fort Peck Reach. *Journal of Hydraulic Engineering*, 130(4), pp.279–292.

Ferrick, M.G. & Calkins, D.J., 1996. Risk-equivalent seasonal discharge programs for ice-covered rivers. , 122(December), pp.442–444.

Ghareh Aghaji Zare, S., A. Moore, S., et al., 2016. alluvial streams. , pp.1306–1327.

Ghareh Aghaji Zare, S., Asce, S.M., et al., 2016. Boundary Shear Stress in an Ice-Covered River during Breakup. , 142(4), pp.1–14.

Ghareh Aghaji Zare, S. et al., 2013. ESTIMATING THE INFLUENCE OF RIVER ICE BREAK-UP ON SUSPENDED SEDIMENT TRANSPORT USING ACOUSTIC TECHNIQUES. *21st Canadian Hydrotechnical Conference*, pp.1–10.

Ghareh Aghaji Zare, S. et al., 2014. Influence of river ice break-up on stream hydraulics and sediment transport. *River Flow 2014 – Schleiss et al. (Eds)*, pp.951–959.

Hammar, L. et al., 2002. A LABORATORY STUDY ON FREEZEUP ICE RUNS IN RIVER. , (December).

Härer, S. et al., 2013. PRACTISE – Photo Rectification And ClassificaTIon SoftwarE (V.1.0). *Geosci. Model Dev*, 6, pp.837–848. Available at: www.geosci-model-dev.net/6/837/2013/.

Hicks, F., 2009. An overview of river ice problems: CRIPE07 guest editorial. *Cold Regions Science and Technology*, 55(2), pp.175–185. Available at: http://dx.doi.org/10.1016/j.coldregions.2008.09.006.

Holland, K.T. et al., 1997. Practical use of video imagery in nearshore oceanographic field studies. *IEEE Journal of Oceanic Engineering*, 22(1), pp.81–91.

Huang, T.S., 1997. Computer Vision: Evolution and Promise. *University of Illinois at Urbana-Champaign*.

Jędrzychowski, K. & Kujawski, A., 2014. Method of image analysis in the process of assessment of ice occurrences. *ZESZYTY NAUKOWE Akademia Morska w Szczecinie*, 37(109), pp.45–49.

Kaufmann, V., 2012. The evolution of rock glacier monitoring using terrestrial photogrammetry: The example of Ausseres hochebenkar rock glacier (Austria). *Austrian Journal of Earth Sciences*, 105(2), pp.63–77.

Keenan, T.F. et al., 2014. Tracking forest phenology and seasonal physiology using digital repeat photography: A critical assessment. *Ecological Applications*, 24(6), pp.1478–1489.

Kerr, D.J., Shen, H.T. & Daly, S.F., 2002. Evolution and hydraulic resistance of anchor ice on gravel bed. *Cold Regions Science and Technology*, 35(2), pp.101–114.

Lind, L., Nilsson, C. & Weber, C., 2014. Effects of ice and floods on vegetation in streams in cold regions: Implications for climate change. *Ecology and Evolution*, 4(21), pp.4173–4184.

Major, J.J. et al., 2009. Monitoring lava-dome growth during the 2004-2008 Mount St. Helens, Washington, eruption using oblique terrestrial photography. *Earth and Planetary Science Letters*, 286(1-2), pp.243–254. Available at: http://dx.doi.org/10.1016/j.epsl.2009.06.034.

Messerli, A. & Grinsted, A., 2015. Image georectification and feature tracking toolbox: ImGRAFT. *Geoscientific Instrumentation, Methods and Data Systems*, 4(1), pp.23–34.

Michel, P., Mathieu, R. & Mark, A.F., 2010. Spatial analysis of oblique photo-point images for quantifying spatio-temporal changes in plant communities. *Applied Vegetation Science*, 13(2), pp.173–183.

Moore, S.A. et al., 2013. Monitoring suspended sediment under ice using acoustic instruments : presentation of measurements made during breakup. *CGU HS Committee on River Ice Processes and the Environment 17th Workshop on River Ice Edmonton, Alberta*.

Niraula, R.R. et al., 2013. Measuring impacts of community forestry program through repeat photography and satellite remote sensing in the Dolakha district of Nepal. *Journal of Environmental Management*, 126, pp.20–29. Available at: http://dx.doi.org/10.1016/j.jenvman.2013.04.006.

P.A. Chambers, G.J. Scrimgeour, A. Pietroniro, J.M. Culp, I.L., 1993. Oxygen Modelling Under River Ice Covers. , pp.235–260.

Pawlowicz, R., 2003. Quantitative visualization of geophysical flows using low-cost oblique digital time-lapse imaging. *IEEE Journal of Oceanic Engineering*, 28(4), pp.699–710.

Pip, E., 1992. The ecology of subarctic molluscs in the lower Nelson river system, manitoba, Canada. *Journal of Molluscan Studies*, 58(2), pp.121–126.

Prowse, T.D., 2001. RIVER-ICE ECOLOGY.I: HYDROLOGIC, GEOMORPHIC, AND WATER-QUALITY ASPECTS By Terry D. Prowse1 ABSTRACT: *Journal of cold regions engineering*, 15(March), pp.330–337.

Prowse, T.D. & Beltaos, S., 2002. Climatic control of river-ice hydrology: A review. *Hydrological Processes*, 16(4), pp.805–822.

Ranjie, H.O.U. & Huimin, L.I., 1987. Modelling of BOD-DO dynamics in an ice-covered river in Northern China. , 21(3), pp.247–251.

Ray, N. & Saha, B.N., 2006. Edge sensitive variational image thresholding. *Proceedings - International Conference on Image Processing, ICIP*, 6.

Schmidt, M. et al., 2015. Multi-resolution time series imagery for forest disturbance and regrowth monitoring in Queensland, Australia. *Remote Sensing of Environment*, 158, pp.156–168. Available at: http://dx.doi.org/10.1016/j.rse.2014.11.015.

Shen, H.T., 2003. Research on River Ice Processes : Progress and Missing Links. *Journal of Cold Regions Engineering*, 17(December), pp.135–142.

Smith, D.G., 1979. Effects of channel enlargement by river ice processes on bankfull discharge in Alberta, Canada. *Water Resources Research*, 15(2), pp.469–475.

Smith, D.G. & Pearce, C.M., 2002. Ice jam-caused fluvial gullies and scour holes on northern river flood plains. *Geomorphology*, 42(1-2), pp.85–95.

Sonnentag, O. et al., 2012. Digital repeat photography for phenological research in forest ecosystems.

Agricultural and Forest Meteorology, 152(1), pp.159–177. Available at: http://dx.doi.org/10.1016/j.agrformet.2011.09.009.

Sui, J. et al., 2002. Field Investigation of Frazil Jam Evolution: A Case Study. *Journal of Hydraulic Engineering*, 128(8), pp.781–787. Available at: http://ascelibrary.org/doi/10.1061/(ASCE)0733-9429(2002)128:8(781).

Sun, Z. & Shen, H.T., 1988. A field investigation of frazil ice jam in Yellow River. *Proceedings of the 5th Workshop on Hydraulics of River Ice/Ice Jams, June, Winnipeg, Manitoba*, pp.157–175.

Tang, G. et al., 2016. Modelling and Analysis of Hydrodynamics and Water Quality for Rivers in the Northern Cold Region of China. *International Journal of Environmental Research and Public Health*, 13(4), p.408. Available at: http://www.mdpi.com/1660-4601/13/4/408.

Tao, H. & Li, S., 2016. Dynamics of Ice Jam Formation and Release. , (52), pp.25–32.

Thung, K.-H.T.K.-H. & Raveendran, P., 2009. A survey of image quality measures. *Technical Postgraduates (TECHPOS), 2009 International Conference for*, pp.1–4. Available at: http://ieeexplore.ieee.org/lpdocs/epic03/wrapper.htm?arnumber=5412098.

Treiber, M.A., 2013. *Optimization for Computer Vision*, Available at: http://link.springer.com/10.1007/978-1-4471-5283-5.

Wang, L.K., Yang Chih Ted & Mu-Hao SWang, 2016. *Advances in Water Resources Management*,

Westoby, M.J. et al., 2012. "Structure- from- Motion" photogrammetry: A low- cost, effective tool for geoscience applications. *Geomorphology*, 179, pp.300–314.

Zare, S.G.A. et al., 2014. Influence of river ice break-up on stream hydraulics and sediment transport. , pp.951–959.

Zhou, L. et al., 2013. Modeling winter wheat phenology and carbon dioxide fluxes at the ecosystem scale based on digital photography and eddy covariance data. *Ecological Informatics*, 18, pp.69–78. Available at: http://dx.doi.org/10.1016/j.ecoinf.2013.05.003.

Zier, J.L. & Baker, W.L., 2006. A century of vegetation change in the San Juan Mountains, Colorado: An analysis using repeat photography. *Forest Ecology and Management*, 228(1-3), pp.251–262.

Zare, S.G.A. et al., 2014. Influence of river ice break-up on stream hydraulics and sediment transport. , pp.951–959.

Zhou, L. et al., 2013. Modeling winter wheat phenology and carbon dioxide fluxes at the ecosystem scale based on digital photography and eddy covariance data. *Ecological Informatics*, 18, pp.69–78. Available at: http://dx.doi.org/10.1016/j.ecoinf.2013.05.003.

Zier, J.L. & Baker, W.L., 2006. A century of vegetation change in the San Juan Mountains, Colorado: An analysis using repeat photography. *Forest Ecology and Management*, 228(1-3), pp.251–262.